Adsorption and Structure of Argon in Activated Porous Carbons

Benoit Coasne

Molecular Simulation
Journal of
Experimental Nanoscience

Taylor & Francis
Taylor & Francis Group

Adsorption and Structure of Argon in Activated Porous Carbons

Journal:	*Molecular Simulation/Journal of Experimental Nanoscience*
Manuscript ID:	GMOS-2005-0091.R1
Journal:	Molecular Simulation
Date Submitted by the Author:	15-Feb-2006
Complete List of Authors:	Coasne, Benoit; CNRS and Universite Montpellier 2, LPMC
Keywords:	Adsorption, Structure, Porous carbons

Adsorption and Structure of Argon in Activated Porous Carbons

Benoit Coasne[a,*], Keith E. Gubbins[b], Francisco R. Hung[b,c] and Surendra K. Jain[b]

[a] *Laboratoire de Physicochimie de la Matière Condensée, CNRS (UMR 5617) and Université Montpellier 2, Montpellier, France;* [b] *Center for High Performance Simulations and Department of Chemical and Biomolecular Engineering, North Carolina State University, Raleigh, USA;* [c] *Department of Chemical and Biological Engineering, University of Wisconsin, Madison, USA.*

[*] To whom correspondence should be addressed. E-mail: bcoasne@lpmc.univ-montp2.fr.

Phone: +33 4 67 14 33 78. Fax: +33 4 67 14 42 90.

Abstract. Molecular simulations are used to investigate the adsorption and structure of argon in ordered and disordered models of porous carbons. The ordered porous carbon (model A) is an assembly of regular slit pores of different sizes, while the disordered porous carbon (model B) is a structural model that reproduces the complex pore shape and pore connectivity of saccharose-based porous carbons. The same pore size distribution is used for models A and B so that we are able to estimate, for similar confinement effects, how the disorder of the porous material affects the adsorption and structure of the confined fluid. Adsorption of argon at 77.4 K in the two models is studied using Grand Canonical Monte Carlo simulations. The structure of the confined fluid is analyzed using crystalline bond order parameters and positional or bond orientational pair correlation functions. The filling pressure for the assembly of slit pores is much lower than that for the disordered porous carbon. It is also found that the isosteric heat of adsorption for the ordered porous model overestimates that for the disordered porous model. The results suggest that the agreement between models A and B would be improved if the same density of carbon atoms was used in these two models. Strong layering of Ar is observed at all pressures for model A. The confined phase is composed of liquid-like layers at low pressures, which crystallize into well-defined hexagonal 2D crystals after complete filling of the pores. The structure of argon in the disordered porous carbon strongly departs from that in the slit pore model. Athough its structure remains liquid-like overall, argon confined in model B is composed of both crystalline clusters and amorphous (solid or liquid) nano-domains.

INTRODUCTION

Activated carbons are porous solids with pores having a width of several angstroms. These materials are used in industrial applications as adsorbents for gas separation, air purification, solvent recovery, etc. [1,2,3,4]. From a fundamental point of view, activated porous carbons are used to investigate the effect of confinement, reduced dimension, and surface forces on the phase behavior of fluids [5,6]. Activated porous carbons are obtained by carbonization and chemical or physical activation of some organic precursor (polymer, coconut shell, saccharose, wood, pitch, etc.). The morphological (pore shape) and topological (connected or unconnected pores) features of these materials depend on the conditions of the activation process and on the initial precursor [1,4]. Samples that are obtained from graphitizable precursors such as polymers or pitch fibers are made up of graphene microcrystals [7,8,9,10]; the porosity in these materials consist of defective slit pores that are located between the graphene sheets. On the other hand, samples that are obtained from non-graphitizable precursors such as saccharose exhibit highly disordered pores that are connected [1,4,11].

In most theoretical and molecular simulation studies on fluids confined in porous carbons, the adsorbent is modeled as an assembly of unconnected slit pores having structureless walls (i.e., without surface corrugation). Experimental data of adsorption in porous carbons are usually analyzed on the basis of such a simple model in order to obtain information regarding the pore size distribution, surface area, etc of the real sample [3]. However, it is not clear whether this approximation is justified as most of these adsorbents are made up of connected pores of a complex morphology. Although a few molecular simulation studies have considered models of porous carbons with surface defects or disorder [11,12,13,14,15,16], the effect of pore shape and pore connectivity on the thermodynamics and structure of fluids confined in these materials remains to be clarified. Recent progress in modelling of porous carbons has been achieved through the use of Reverse Monte Carlo (RMC) algorithms [17]. Gubbins and coworkers have applied this technique to obtain structural models of saccharose based porous carbons [11,15,18,19]. Simulated transmission electron microscopy, gas adsorption, and

microcalorimetry for these realistic models were found to be in good agreement with experimental data [16].

In this paper, we report a molecular simulation study of adsorption of argon in ordered and disordered models of activated porous carbons. The ordered porous carbon (model A) is an assembly of regular slit nanopores of different sizes; this model is supposed to be a reasonable approximation for activated carbons obtained from graphitizable precursors. The disordered porous carbon (model B) is a structural model of saccharose-based porous carbon, which was obtained using the RMC method [15]. The disorder in terms of pore shape and pore connectivity in this model is representative of real materials [15]. The same pore size distribution is used for models A and B, so that the comparison between the two set of results allows us to estimate, for similar confinement effects, how the disorder of the porous material affects the adsorption and structural properties of the adsorbate.

Adsorption of argon in the ordered and disordered models of porous carbons was studied using Grand Canonical Monte Carlo (GCMC) simulations. Both the adsorption isotherm (adsorbed amount as a function of the gas pressure) and the isosteric heat of adsorption (differential enthalpy of adsorption as a function of the filling fraction) were calculated in the simulations. The structure of the confined fluid was also determined in the course of the simulations using crystalline bond order parameters and positional or bond orientational pair correlation functions. This paper is organized as follows. The ordered and disordered models of porous carbons and the simulation techniques are described in the second section. Adsorption and structure of argon in the two models of activated porous carbon are discussed in the third section. Concluding remarks and suggestions for future work are presented in the last section of the manuscript.

MODELS AND SIMULATION METHODS

Ordered porous carbons

Ordered porous carbons (model A) were modeled as an assembly of unconnected slit pores having a regular width. The graphite walls in this model are structureless, i.e. without atomic surface corrugation; this approximation is expected to be reasonable for argon as the size of this adsorbate, σ ~ 3.405 Å, is much larger than the spacing between carbon atoms in graphite, D ~ 1.4 Å. The square section of the parallel walls were chosen equal to 20σ × 20σ, which corresponds to 68.1 Å × 68.1 Å. The interaction between the adsorbate atoms and each pore wall was determined using the Steele '10-4-3' potential [20,21]:

$$U_{wf}(z) = 2\pi\rho_w\varepsilon_{wf}\sigma_{wf}^2\Delta\left[\frac{2}{5}\left(\frac{\sigma_{wf}}{z}\right)^{10} - \left(\frac{\sigma_{wf}}{z}\right)^{4} - \left(\frac{\sigma_{wf}^4}{3\Delta(z+0.61\Delta)^3}\right)\right] \quad (1)$$

where z is the distance between the argon atom and the graphite surface. Δ = 3.35 Å is the separation between graphite layers and ρ_w = 0.114 Å^{-3} the atomic density of graphite layers. ε_{wf} and σ_{wf} were calculated by combining the Lennard – Jones parameters for the carbon/carbon [20] and argon/argon [22] interactions using the Lorentz-Berthelot rules [23] (see Table 1).

Disordered porous carbons

The disordered porous carbon (model B) used in this work is shown in Figure 1. This structural model of activated porous carbon obtained after carbonization and activation of pure saccharose has been built by Jain et al. using a constrained RMC technique. This reconstruction method consists of generating atomic configurations that match the structural properties of the real system [17]. The quantity to be minimized in the course of the simulation is:

$$\chi^2 = \sum_{i=1}^{n\exp}\left[S_{sim}(q_i) - S_{\exp}(q_i)\right]^2 \quad (2)$$

where S_{sim} is the simulated structure factor and S_{exp} is the experimental structure factor. Changes in the

atomic configurations are accepted or rejected according to the Metropolis acceptance probability:

$$P_{acc} = \min\left[1, \exp\left\{-\frac{1}{T_\chi}\left(\chi^2_{new} - \chi^2_{old}\right)\right\}\right] \quad (3)$$

where T_χ is a weighting parameter. The uniqueness of structures determined by the RMC method has been questioned in the literature [24]. If many body forces are important in the system (as for carbon materials in which chemical bonding is involved), then it is necessary to include some constraints, representative of these forces, in the RMC method to completely specify the system. Following the previous work by Pikunic et al. [11], appropriate constraints were used to build the realistic model of activated porous carbon considered in this work. The first constraint is that the fraction of atoms in the model having sp^2 hybridization (i.e., coordination number of 3) is centered about this same fraction determined from the experimental composition. The second constraint is that the average C-C-C bond angle, θ, must be equal to $2\pi/3$, as expected for sp^2 hybridization. In the RMC simulation, the difference between the experimental and simulated pair correlation function are simultaneously minimized with the two constraints:

$$\chi^2 = \sum_{i=1}^{n_{\exp}}\left[g_{sim}(r_i) - g_{\exp}(r_i)\right]^2, \quad \delta^2 = \left[\left(\frac{N_3}{N}\right)_{sim} - \left(\frac{N_3}{N}\right)_{target}\right]^2, \quad \psi^2 = \frac{1}{n}\sum_{\theta_i=1}^{n_\theta}\left[\cos(\theta_i) - \cos\left(\frac{2\pi}{3}\right)\right]^2 \quad (4)$$

where $g(r)$ is the radial distribution function for carbon atoms in the material.

In order to improve the quality of the sampling in the RMC simulation, the method was combined with a simulated annealing technique. The latter is a minimization technique that consists of first melting at high temperature the structure to be optimized and then slowly lowering the temperature. Starting with a random initial structure at high temperature, the system runs at this temperature for a large number of moves until it reaches equilibrium; each move consists of randomly selecting and displacing a C atom to

a new position. Then, the temperature is decreased and the system is again allowed to equilibrate. The simulation is complete when no further change is observed upon decrease of the temperature. Full details of the simulation techniques can be found in Refs. [11] and [15].

Grand Canonical Monte Carlo simulations

Argon adsorption in the different models of activated porous carbons was simulated using the GCMC algorithm. The GCMC technique is a stochastic method that simulates a system having a constant volume V (the pore with the adsorbed phase), in equilibrium with an infinite fictitious reservoir of particles imposing its chemical potential μ and its temperature T [25,26,27]. For different values of μ, the absolute adsorption isotherm is determined as an ensemble average of the number of adsorbed atoms *versus* the pressure of the gas reservoir P (the latter is obtained from the chemical potential according to the equation of state for an ideal gas [28]). The adsorption and desorption processes are simulated by increasing and decreasing the chemical potential of the reservoir, respectively; the final configuration obtained from the simulation for a particular chemical potential is the initial configuration for the next point. Periodic boundary conditions were applied for both models A and B in order to avoid finite-size effects. The Ar/Ar interactions were calculated using Lennard-Jones potentials with the parameters reported in Table 1. As mentioned above, interactions between Ar and the slit pore walls for model A were calculated using the 10 – 4 – 3 Steele potential given by equation (1). The interaction of argon atoms with the carbon atoms of the disordered porous material were modeled using a Lennard-Jones potential; the fluid/fluid and fluid/wall parameters were the same as those used for the slit pore model (Table 1). In order to accelerate the simulations in the case of model B, the adsorbate/substrate interaction was calculated by using an energy grid [29]; the potential energy is calculated at each corner of each elementary cube (about $0.025 \times 0.025 \times 0.025$ nm^3). An accurate estimation of the energy is then obtained by a linear interpolation of the grid values. This procedure enables simulation of adsorption in nanoporous media of complex morphology and/or topology without a direct summation over matrix species in the course of GCMC runs [30,31,32,33]. Typical GCMC runs consists of an

equilibration stage of at least 10^5 Monte Carlo steps per particle to equilibrate the system, followed by a production stage of 2.10^5 Monte Carlo steps per particle to obtain averaged data.

RESULTS AND DISCUSSION

Adsorption isotherm and isosteric heat

Argon adsorption in graphite slit pores was studied for 19 pore sizes ranging from H = 6.0 to 15.0 Å; the width difference between two consecutive pore sizes was 0.5 Å. This width range was selected as it covers the pore size distribution for the disordered carbon (see Figure 1). Ar adsorption isotherms at 77.4 K are reported in Figure 2 for the slit pores H = 8, 10, 12 and 15 Å. Adsorbed amounts have been normalized to the maximum number of adsorbed atoms at $P = P_0$. The filling of the slit pores H = 8 and 10 Å occurs at $P = 2.0 \times 10^{-7}\ P_0$ and $1.0 \times 10^{-5}\ P_0$, respectively. These two slit pores accommodate one layer of confined argon after complete filling of the porosity. On the other hand, the adsorption isotherms for the slit pores H = 12 and 15 Å exhibits several steps, which correspond to the filling of different number of layers. For instance, the filling for H = 12 Å starts at $P = 1.0 \times 10^{-4}\ P_0$ with the formation of two layers of confined fluid and ends at $P = 2.0 \times 10^{-3}\ P_0$ with the formation of a third layer within the pore. The filling for H = 15 Å involves a three stage – process with the filling of 3, 4 and 5 layers of argon at $P = 2.0 \times 10^{-4}\ P_0$, $5.0 \times 10^{-3}\ P_0$ and $2.0 \times 10^{-2}\ P_0$, respectively. The dependence of the nature of the filling mechanism on the pore width has been addressed in several recent papers [34,35,36,37]. As expected for adsorption of simple adsorbates in graphite slit pores, we found in general that the filling pressure increases as the pore width increases. However, some exceptions to this rule were observed; for instance, the filling pressure for H = 6 Å, $P = 2.0 \times 10^{-4}\ P_0$, is much larger than that for H = 8 Å, $P = 2.0 \times 10^{-7}\ P_0$, although these two pores accommodate the same number of layers. This result is due to the fact that the wall/fluid interaction energy of an atom in the center of the pore is smaller for H = 6 Å than for H = 8 Å because the atom feels more the repulsive part of the wall/fluid potential in the first case than in the second one (see Ref. [38] for a detailed discussion on the optimal

pore width for a given number of layers).

The Ar adsorption isotherm at 77.4 K for the disordered porous carbon (model B) is shown in Figure 2. We also report the Ar adsorption isotherm for an assembly of unconnected slit pores (model A) having the same pore size as that of model B. The adsorbed amount $N(P/P_0)$ for model A was calculated at a given pressure P/P_0 by:

$$N(P/P_0) = \int_0^\infty n(H, P/P_0)\, p(H)\, dH \qquad (5)$$

where $p(H)$ is the pore size distribution (see Figure 1) and $n(H, P/P_0)$ the adsorbed amount in the pore of width H. We used a discrete sum in equation (5) instead of an integral, due to the use of a finite number of pore sizes. All the adsorption isotherms shown in Figure 2 have been normalized to the number of adsorbed atoms at $P = P_0$. Both the adsorption isotherms for models A and B are characteristic of adsorption in microporous adsorbents (type I in the IUPAC classification [3]); the filling of the porosity is a reversible process that occurs at very low pressures. The filling of the disordered porous carbon occurs on a range of pressure from $P = 10^{-4}\ P_0$ up to $P = 4.0 \times 10^{-2}\ P_0$, while the filling of the slit pores spans over a much larger pressure range from $P = 10^{-8}\ P_0$ up to $P = 5.0 \times 10^{-3}\ P_0$. The pressure at which half of the porosity is filled is lower for model A, $P = 5.0 \times 10^{-5}\ P_0$, than for model B, $P = 10^{-2}\ P_0$. It is also found that, at all pressures, the adsorbed amount for the assembly of slit pores is larger than that for the disordered carbon. These last results show that the slit pore model significantly understimates the filling pressure of the disordered porous carbon. This finding is in full agreement with our previous work on nitrogen adsorption at 77 K in ordered and disordered porous carbons [13]. As noted in Ref. [13], the difference between the two pore models can be explained by the larger carbon density used in model A, $\rho = 0.114$ Å^{-3}, than that used in model B, $\rho = 0.036$ Å^{-3}. We expect that the agreement between the adsorption isotherms obtained for the ordered and disordered porous carbons can be improved if the same density of carbon atoms is used. However, we have not

attempted to do that because of the important differences in the behavior of the isosteric heat obtained from both models (see below), which will not be eliminated by simply adjusting the density of carbon atoms.

The isosteric heat of adsorption, Q_{st}, as a function of the filling fraction is shown in Figure 3 for the assembly of slit pores and the disordered porous carbon. The latter quantity was calculated in the GCMC simulations from the fluctuations over the energy, *U*, and number of particles, *N*, according to the following formula [25]:

$$Q_{st} = k_B T - \frac{\partial \langle U \rangle}{\partial \langle N \rangle} \sim k_B T - \frac{\langle UN \rangle - \langle U \rangle \langle N \rangle}{\langle N^2 \rangle - \langle N \rangle^2} \qquad (6)$$

For all filling fractions, the isosteric heat of adsorption for the disordered porous carbon is lower than that for the assembly of slit pores. Q_{st} for the slit pore model exhibits a maximum value for $N/N_0 \sim 0.07$ as it first increases from 10 kJ/mol up to 22 kJ/mol and then decreases down to 16 kJ/mol. In contrast, the isosteric heat of adsorption curve for model B is characteristic of adsorption in heterogeneous porous systems as Q_{st} decreases with increasing the filling fraction. This feature is in qualitative agreement with microcalorimetry measurements on disordered porous carbons [16], showing that model B reproduces in a more realistic way the adsorption properties of real porous carbons than model A. We also report in Figure 3 the fluid/wall and fluid/fluid contributions to the total isosteric heat of adsorption for both models A and B. The wall/fluid contribution represents at all filling fractions more than 50% of the total isosteric heat of adsorption. This contribution shows a generally decreasing tendency with increasing N/N_0 as sites of high energy are first filled followed by sites of lower energy. In contrast, the fluid/fluid contribution increases with increasing N/N_0 as the fluid/fluid interaction energy becomes larger. However, it is found that this fluid/fluid contribution slightly decreases at very large filling fractions ($N/N_0 \geq 0.9$) for model B; this result is due to the fact that adsorbed atoms feel the repulsive part of the fluid/fluid interaction at high density (compressibility limit of the fluid). We could not check

this effect of the short range repulsion for model A as fluctuations over the energy and the number of adsorbed atoms at high density were not large enough to get reasonable estimates of the isosteric heat of adsorption. The fluid/fluid contribution of Q_{st} for the slit pore model is always larger than that for the disordered porous carbon. This result is due to the slit pore geometry, which allows the formation of well-structured layers of argon (see below) that are more stable than disordered adsorbate structures. It is found that the fluid/wall contribution to the isosteric heat of adsorption for model A also overestimates that for model B. As mentioned above, this result can be explained by the larger density of carbon walls used in model A, which leads to larger wall/fluid interaction energy.

Structure of the confined fluid

The structure of the confined fluid was analyzed for both models A and B using crystalline bond order parameters, and positional and bond orientational pair correlation functions. Three different sizes, H = 7, 11 and 14 Å, were considered for the slit pore model as they correspond to the smallest, mean, and largest pore size in the disordered porous carbon, respectively. Density profiles of Ar confined at T = 77.4 K are shown in Figure 4 for the slit pores H = 7, 11 and 14 Å. Here z* and ρ* are respectively the reduced distance from the center of the pore and the reduced density with respect to σ. For each pore, we report both the density profile at the onset of pore filling and at the saturated vapor pressure. Significant layering of Ar was observed for all the slit pores as 2D layers are separated by a minimum value of the density, ρ* = 0. This result is due to the strong interaction between argon and the attractive pore walls, which leads to the ordering of the adsorbed phase. For all pressures, the slit pore H = 7 and 11 Å accommodate one and two layers, respectively. On the other hand, the slit pore H = 14 Å accommodates two layers at low pressures and three layers after pore filling. In the latter case, it is found that the peak amplitude for the inner layer is lower than that for the two contact layers (see Figure 4). This result shows that the contact layers are more ordered than the inner layer, due to its stronger interaction with the pore wall. A detailed study of the structure of argon confined in the slit pore H = 14 Å is reported in what follows but similar results were found for the slit pores H = 7 and 11 Å. Following

previous molecular simulation studies on simple fluids in slit pores, the structure of confined argon was investigated by calculating for each layer of adsorbate the in-plane 2D positional g(r) and bond-orientational $G_6(r)$ pair correlation functions [39,40,41,42,43]. The latter measures for each layer *i* the correlations between the local order parameter $\Psi_{6,j}(r)$ at two positions separated by a distance *r*:

$$G_{6.i}(r) = \left\langle \Psi^{*}_{6,i}(0)\Psi_{6,i}(r) \right\rangle \quad (7)$$

$\Psi_{6,i}(r)$ is the hexagonal bond-order parameter of a particle located at a position **r** in the layer *i* [44,45]:

$$\Psi_{6,i}(\mathbf{r}) = \frac{1}{N_b}\sum_{k=1}^{N_b} \exp\left(i6\theta_k\right) \quad (8)$$

where θ_k is the orientation of the bond angle between the central molecule and each of its N_b nearest neighbors. Correlations within each layer were determined up to a distance of half the size of the simulation box. The g(r) and $G_6(r)$ functions for the contact layer of argon at $P = 2.0 \times 10^{-4}\ P_0$ in the slit pore H = 14 Å are shown Figure 5 and Figure 6. We report only pair correlation functions for the contact layers as the pore H = 14 Å accommodates only two contact layers at this pressure located at the onset of pore filling. We also show in Figure 5 and Figure 6 the g(r) and $G_6(r)$ functions for the contact and inner layers of argon in the same slit pore at $P = P_0$. At $P = 2.0 \times 10^{-4}\ P_0$, the confined layers exhibit a fluid-like behavior as revealed by the g(r) function, which is characteristic of a phase having short-range positional order. This result is confirmed by the very fast decay observed in the $G_6(r)$ function; such a decay is typical of 2D fluid phases, which have short-range orientational order. In contrast, both the contact and inner layers at $P = P_0$ are 2D hexagonal crystals with long-range positional order as can be seen from the features of the g(r) function for this pressure (Figure 5); (i) the amplitude between the first and the second peak is close to 0, (ii) the second peak is split into two secondary peaks, and (iii) the third peak presents a shoulder on its right side. Moreover, the $G_6(r)$ functions at this pressure have a constant average value as expected for hexagonal crystal layers with long-range orientational order

(Figure 6). Analysis of the in-plane 2D pair correlation functions g(r) and $G_6(r)$ was confirmed by calculating for each adsorbate layer *i* the 2D bond-order parameters $\Phi_{6,i}$. We determined $\Phi_{6,i}$ as the average value of the local order parameter $\Psi_{6,i}(r)$ over the entire layer [44,45]:

$$\Phi_{6,i} = \frac{\left|\int \Psi_{6,i}(\mathbf{r})\, d\mathbf{r}\right|}{\int d\mathbf{r}} \qquad (9)$$

$\Phi_{6,i}$ is 1 for a perfect crystal layer having a hexagonal structure (i.e., triangular symmetry) and close to 0 for a liquid layer. At $P = 2.0 \times 10^{-4}\ P_0$, $\Phi_6 = 0.14$ as expected for confined layers having short-ramge orientational order. On the other hand, $\Phi_6 = 0.81$ for the contact and inner layers at $P = P_0$, which confirms that the adsorbate layers have a hexagonal crystal structure with, however, some defects. These results show that argon confined in slit pores at the saturated vapor pressure has a crystalline structure at $T = 77.4$ K, that is lower than the bulk freezing temperature, $T = 83$ K. This finding is consistent with previous molecular simulation studies, which have shown that simple fluids confined in strongly attractive pores crystallize at higher temperature than the bulk [6,39,40,46].

The positional pair correlation function g(r) for Ar confined at 77.4 K in the disordered porous carbon (model B) is shown in Figure 7 for three different pressures $P = 3.0 \times 10^{-5}\ P_0$, $3.0 \times 10^{-3}\ P_0$, and P_0. The filling fractions N/N_0 for these three pressures are 0.05, 0.50 and 1.00, respectively. In contrast to the in-plane 2D g(r) functions used for the slit pore geometry, the functions shown in Figure 7 are 3D pair correlations functions, as no layered structure was observed for argon in the disordered porous carbon (the *x*, *y*, and *z* directions are equivalent for this porous material). For all pressures, the g(r) function of argon confined in model B is characteristic of liquid-like structures as only short – range positional order is observed. It is found that the positional correlations are limited to the first nearest neighbors for the lowest pressure, while they extend to the second and third nearest neighbors for $P = 3.0 \times 10^{-5}\ P_0$ and $3.0 \times 10^{-3}\ P_0$. This change in the range of the correlations indicates that the confined phase presents more short-range structure with increasing filling fraction, although it remains liquid-like overall.

The structure of argon confined in the disordered porous carbon was further characterized by determining its degree of crystalline order. Global crystalline order parameters are not suitable for studying the structure of fluids in the complex porous carbon as the large degree of disorder of the sample prevents the positional and orientational order of the confined phase from being coherent [47]. Thus, instead of global parameters, we used a local order parameter proposed by Ten Wolde et al. [47] to calculate the percentage of atoms that are crystal-like. For each atom *i* of the confined phase, we calculated the 13 normalized parameters $\tilde{q}_{6m}(i)$ that are defined as:

$$\tilde{q}_{6m}(i) = \frac{A}{N_b(i)} \sum_{j=1}^{N_b(i)} Y_{6m}\left(\theta_{ij}, \phi_{ij}\right) \text{ with } m \in [-6,6] \qquad (10)$$

where θ_{ij} and ϕ_{ij} are the polar and azimuthal angles giving the orientation of the vectors joining the atom *i* and each of its $N_b(i)$ neighbors *j*. Y_{6m} are spherical harmonics and A the normalization constant. $\tilde{q}_{6m}(i)$ is a local quantity that depends only on atom *i* and its neighbors *j*. For each pair of nearest neighbors, Ten Wolde et al. defined the following scalar product [47]:

$$\mathbf{q}_6(i) \cdot \mathbf{q}_6(j) = \sum_{m=-6}^{6} \tilde{q}_{6m}(i) \tilde{q}_{6m}(j)^* \qquad (11)$$

Atoms *i* and *j* can be considered "connected" in a coherent manner if the product $\mathbf{q}_6(i) \cdot \mathbf{q}_6(j)$ is larger or equal to 0.5. Ten Wolde et al. have shown that an atom *i* in a 3D environment is crystal-like if it is connected in a coherent manner to at least 7 of its nearest neighbors; this definition ensures that liquid and bcc or fcc crystal structures are unambiguously distinguished [47].

The distribution of the number of connections per Ar particle in the disordered porous carbon was determined for several pressures, $P = 3.0 \times 10^{-5}\ P_0$, $P = 3.0 \times 10^{-3}\ P_0$, and $P = P_0$, from the number of connections for which $\mathbf{q}_6(i) \cdot \mathbf{q}_6(j) \geq 0.5$ (Figure 7). The average number of connections per particle

increases with increasing the pressure from 0.6 at $P = 3.0 \times 10^{-5}\ P_0$ up to 6.7 at $P = P_0$. At the lowest pressure, the confined phase is composed only of liquid-like particles (number of connections < 7). In contrast, the confined phase for $P = 3.0 \times 10^{-3}\ P_0$ and P_0 is composed of both crystal-like and liquid-like adsorbed atoms. We note that, even at the saturating pressure, the average number of connections per particle is much lower than the values expected for FCC and BCC bulk crystals (number of connections ~ 12 and 13, respectively [47]). This result is due to the confinement and the disorder of the porous material, which prevent the formation of any bulk-like regular crystal.

The percentage of Ar atoms that are crystal-like is 0% for $P = 3.0 \times 10^{-5}\ P_0$, 6% for $P = 3.0 \times 10^{-3}\ P_0$, and 54% for $P = P_0$. This result indicates that the confined phase for the two highest pressures corresponds to a mixture of crystalline clusters and amorphous (liquid or solid) regions. This finding strongly departs from what is observed for the slit geometry, where the pore accommodates layers of adsorbate having a well-defined crystalline structure. Our results for the disordered porous carbon are consistent with previous molecular simulations and experiments on molecular fluids in cylindrical silica or carbon pores [48,49,50,51], which have found that the confined fluid does not crystallize but forms an inhomogeneous phase composed of nanocrystallites and amorphous regions. We report in Figure 8 typical atomic configurations of argon confined in the disordered porous carbon at $P = 3.0 \times 10^{-3}\ P_0$ and $P = P_0$ in which we distinguish Ar atoms that are crystal-like and liquid-like.

CONCLUSION

This paper reports a molecular simulation study on adsorption of argon in ordered (model A) and disordered (model B) activated porous carbons. Model A is an assembly of regular slit nanopores, which is representative of graphitizable porous carbons. Model B is a realistic sample of porous carbons obtained from Reverse Monte Carlo; the complex pore shape and pore connectivity of this structural model is representative of materials obtained after carbonization and activation of pure saccharose. Models A and B have the same pore size distribution, which ranges from 6 to 15 Å. Molecular

simulation of argon in these two models of activated porous carbons is used to estimate how the confinement and the disorder of the porous structure affects both the adsorption and the structure of a simple adsorbate. Adsorption of argon at 77.4 K was investigated in the two pore models by means of GCMC simulations. The structure of the confined fluid was analyzed using crystalline bond order parameters and positional or bond orientational pair correlation functions.

Both the Ar adsorption isotherms for the ordered and disordered porous carbon are characteristic of adsorption in microporous adsorbents as the filling mechanism is reversible and occurs at very low pressures. The filling pressure for the assembly of slit pores is found to be much lower than that for the disordered porous carbon, in agreement with our previous work on nitrogen adsorption in similar models of activated porous carbons [13]. It seems that the agreement between models A and B can be improved if the same density of carbon atoms is used for the ordered and disordered models of porous carbons. The isosteric heat of adsorption as a function of the filling fraction exhibits a maximum value for model A, which is not observed for model B. The isosteric heat of adsorption for model B is characteristic of adsorption in heterogeneous porous systems, as it decreases with increasing the filling fraction. It is found that the isosteric heat for the assembly of slit pores is greater than that for the disordered porous carbon. This result can be explained as follows. First, the slit pore geometry allows the formation of well-structured layers of argon, which leads to higher fluid/fluid interactions compared to the disordered porous carbon. In addition, the fluid/wall interaction for the slit pores is greater than that for the complex porous carbon, due to the larger density of the carbon walls used in the first case.

Strong layering of Ar is observed for model A. At low pressures (i.e. at the onset of pore filling), both the positional and bond-orientational pair correlation functions show that the adsorbate is made up of 2D confined layers having a liquid-like structure. However, it is found that these layers transform into 2D hexagonal crystal layers as the pore becomes filled. The structure of argon in the disordered porous carbon strongly departs from that in the slit pores. For all filling fractions, the positional pair correlation function g(r) of Ar confined in this disordered material is characteristic of liquid-like structures as only

short – range positional order is observed. However, except at very low pressures where argon atoms are all liquid-like, the confined phase is a mixture of crystalline clusters and amorphous (solid or liquid) nanodomains. This finding is consistent with previous studies on fluids in cylindrical silica or carbon pores, which have shown that the confined fluid forms an inhomogeneous phase of crystallites and amorphous regions.

Further molecular simulations are needed to corroborate and complete the present study. Starting from well-equilibrated configurations of argon in the disordered porous material, we will investigate the dynamics of the confined phase using Molecular Dynamics simulations for different filling fractions. This will provide useful information regarding the nature of the confined phase, such as its diffusion coefficient and relaxation time. From an experimental point of view, differential scanning calorimetry can be used to corroborate our findings and neutron scattering would allow us to gain insights on the structure and/or the dynamics of the confined phase.

Acknowledgements

We thank the U.S. National Science Foundation for support of this research (grant no. CTS-0211792). This research was performed using supercomputing resources from San Diego Supercomputer Center (NSF/MRAC – CHE050047S), the High Performance Computing Center at North Carolina State University, and the Centre Informatique National de l'Enseignement Superieur at Montpellier (CMC 2017).

[1] Bansal, R. C., Donnet, J. B. and Stoeckli, F. (1988) *Active Carbon* (Marcel Dekker, New York).

[2] Sircar, S., Golden, T. C. and Rao, M. B. (1996) "Activated carbon for gas separation and storage", *Carbon* **34**, 1.

[3] Rouquerol, F., Rouquerol, J. and Sing, K. S. W. (1999) *Adsorption by Powders and Porous Solids* (Academic Press, London).

[4] Bandosz, T. J., Biggs, M. J., Gubbins, K. E., Hattori, Y., Liyama, T., Kaneko, K., Pikunic, J. P. and Thomson, K. T. (2003) "Molecular models of porous carbons", *Chem. Phys. Carbon* **8**, 41.

[5] Gelb, L. D., Gubbins, K. E., Radhakrishnan R. and Sliwinska-Bartkowiak, M. (1999) "Phase separation in confined systems", *Rep. Prog. Phys.* **62**, 1573.

[6] Alba-Simionesco, C., Coasne, B., Dosseh, G., Dudziak, G., Gubbins, K. E., Radhakrishnan, R. and Sliwinska-Bartkowiak, M. (2006) "Effects of confinement on freezing and melting", *J. Phys.: Condens. Matter*, in press.

[7] McEnaney, B. (1988) "Adsorption and structure in microporous carbons", *Carbon* **26**, 267.

[8] March, H. and Walker, P. L. Jr. (1979), In: *Chemistry and Physics of Carbon* (Marcel Dekker, New York) Vol. 15, Chap. 3.

[9] Mays, T. J. (1999) In: *Carbon Materials for Advanced Technologies* (Pergamon, Amsterdam), Chap. 3.

[10] Huang, Z. H., Kang, F., Huang, W., Yang, J. B., Liang, K. M., Cui, M. L. and Cheng, Z. (2002) "Pore structure and fractal characteristics of activated carbon fibers characterized by using HRTEM", *J. Coll. and Interf. Sci.* **249**, 453.

[11] Pikunic, J., Clinard, C., Cohaut, N., Gubbins, K. E., Guet, J. M., Pellenq, R. J. –M., Rannou, I. and Rouzaud, J. –N. (2003) "Structural modeling of porous carbons: constrained reverse Monte Carlo method", *Langmuir* **19**, 8565.

[12] Striolo, A., Gubbins, K. E., Chialvo, A. A. and Cummings, P. T. (2005) "The effect of pore connectivity on water adsorption isotherms in non-activated graphitic nanopores", *Adsorption* **11**, 337.

[13] Coasne, B., Pikunic, J. P., Pellenq, R. J.-M. and Gubbins, K. E. (2003) "Comparison between adsorption in pores of a simple geometry and realistic models of porous materials", *Proc. Mat. Res. Soc.* **P8.5**.

[14] Biggs, M. J., Buts, A. and Williamson, D. (2004) "Molecular simulation evidence for solidlike adsorbate in complex carbonaceous micropore structures", *Langmuir* **20**, 5786.

[15] Jain, S. K., Pikunic, J. P., Pellenq, R. J. –M. and Gubbins, K. E. (2005) "Effects of activation on the structure and adsorption properties of a nanoporous carbon using molecular simulation", *Adsorption* **11**, 355.

[16] Pikunic, J. P., Llewellyn, P., Pellenq, R. J. –M. and Gubbins, K. E. (2005) "Argon and nitrogen adsorption in disordered nanoporous carbons: simulation and experiment", *Langmuir* **21**, 4431.

[17] McGreevy, R. L. and Pusztai, L. (1988) "Reverse Monte Carlo Simulation: A new technique for the determination of disordered structures", *Mol. Sim.* **1**, 359.

[18] Thomson, K. T. and Gubbins, K. E. (2000) "Modeling structural morphology of microporous carbons by reverse Monte Carlo", *Langmuir* **16**, 5761.

[19] Jain, S. K., Fuhr, J., Pellenq, R. J. –M., Pikunic, J. P., Bichara, C. and Gubbins, K. E. (2005) "Stability study of porous carbon structures obtained from reverse Monte Carlo using tight binding and bond order Hamiltonians", *Studies in Surface Science and Catalysis*, in press.

[20] Steele, W. A. (1973) "The physical interaction of gases with crystalline solids", *Surf. Sci.* **36**, 317.

[21] Steele, W. A. (1974) *The Interaction of Gases with Solid* Surfaces (Pergamon Press, Oxford).

[22] Streett, W. B. and Staveley, L. A. K. (1967) "Calculation on a corresponding states basis of the volume change on mixing simple liquids", *J. Chem. Phys.* **47**, 2449.

[23] Rowlinson, J. S. (1982) *Liquids and Liquid Mixtures* (Butterworth Scientific, London).

[24] Evans, R. (1990) "Comment on Reverse Monte Carlo Simulation", *Mol. Sim.* **4**, 409.

[25] Nicholson, D. and Parsonage, N. G. (1982) *Computer Simulation and the Statistical Mechanics of Adsorption* (Academic Press, New York).

[26] Allen, M. P., Tildesley, D. J. (1987) *Computer Simulation of Liquids* (Oxford, Clarendon).

[27] Frenkel, D. and Smit, B. (2002) *Understanding Molecular Simulation: From Algorithms to Applications*, 2nd Ed. (Academic Press, London).

[28] D. A. Kofke (1993) "Direct evaluation of phase coexistence by molecular simulation via integration along the saturation line", *J. Chem. Phys.* **105**, 405.

[29] Pellenq, R. J. –M. and Nicholson, D. (1995) "Grand ensemble Monte Carlo simulation of simple molecules adsorbed in silicalite-I zeolite", *Langmuir* **11**, 1626.

[30] Coasne, B. and Pellenq, R. J. –M. (2004) "A grand canonical Monte Carlo study of capillary condensation in mesoporous media: effect of the pore morphology and topology", *J. Chem. Phys.* **121**, 3767.

[31] Coasne, B., Gubbins, K. E. and Pellenq, R. J. –M. (2004) "A grand canonical Monte Carlo study of adsorption and capillary condensation phenomena in nanopores of various morphologies and topologies: testing the BET and BJH characterization methods", *Part. Part. Syst. Charact. 21*, 149.

[32] Gelb, L. D. and Gubbins, K. E. (1998) "Characterization of porous glasses: simulation models, adsorption isotherms, and the Brunauer-Emmett-Teller analysis method", *Langmuir* **14**, 2097.

[33] Pellenq, R. J. –M. and Levitz, P. E. (2002) "Capillary condensation in a disordered mesoporous medium: a grand canonical Monte Carlo study", *Mol. Sim.* **100**, 2059.

[34] Ayappa, K. G. and Ghatak, C. (2002) "The structure of frozen phases in slit nanopores: A grand canonical Monte Carlo study", *J. Chem. Phys.* **117**, 5373.

[35] Bock, H., Gubbins, K. E. and Ayappa, K. G. (2005) "Solid/solid phase transitions in confined thin films: A zero temperature approach", *J. Chem. Phys.* **122**, 094709.

[36] Patrykiejew, A., Salamacha, L. and Sokolowski, S. (2003) "On the structure of Lennard-Jones fluids confined in crystalline slitlike pores", *J. Chem. Phys.* **118**, 1891.

[37] Camara, L. G. and Bresme, F. (2003) "Molecular Dynamics simulations of crystallization under confinement at triple point conditions", *J. Chem. Phys.* **119**, 2792.

[38] Do, D. D. and Do, H. D. (2003) "Refined method of potential enhancement in the equilibria characterization of activated carbon. Comparison with GCMC and DFT", *Langmuir* **19**, 8302.

[39] Radhakrishnan, R. and Gubbins, K. E. (1999) "Free energy studies of freezing in slit pores: an order parameter approach using Monte Carlo simulation", *Mol. Phys.* **96**, 1249.

[40] Radhakrishnan, R., Gubbins, K. E. and Sliwinska-Bartkowiak, M. (2002) "Global phase diagrams for freezing in porous media", *J. Chem. Phys.* **116**, 1147.

[41] Coasne, B., Czwartos, J., Gubbins, K. E., Hung, F. R. and Sliwinska-Bartkowiak, M. (2004) "Freezing and melting of binary mixtures confined in a nanopore", *Mol. Phys.* **102**, 2149.

[42] Coasne, B., Czwartos, J., Gubbins, K. E., Hung, F. R. and Sliwinska-Bartkowiak, M. (2005) "Freezing of mixtures confined in a slit nanopore", *Adsorption* **11**, 301.

[43] Hung, F. R., Coasne, B., Gubbins, K. E., Santiso, E. E., Siperstein, F. R. and Sliwinska-Bartkowiak, M. (2005) "Molecular modeling of freezing of simple fluids confined within carbon nanotubes", *J. Chem. Phys.* **122**, 144706.

[44] Halperin, B. I. and Nelson, D. R. (1978) "Theory of two dimensional melting", *Phys. Rev. Lett.* **41**, 121; Nelson, D. R. and Halperin, B. I. (1979) "Dislocation – mediated melting in two dimensions", *Phys. Rev. B* **19**, 2457.

[45] Strandburg, K. J. (1988) "Two – dimensional melting", *Rev. Mod. Phys.* **60**, 161.

[46] Radhakrishnan, R., Gubbins, K. E., Watanabe, A. and Kaneko, K. (1999) "Freezing of simple fluids in microporous activated carbon fibers: comparison of simulation and experiment", *J. Chem. Phys.* **111**, 9058.

[47] ten Wolde, P. R., Ruiz-Montero, M. J. and Frenkel, D. (1996) "Numerical calculation of the rate of crystal nucleation in a Lennard-Jones system at moderate undercooling", *J. Chem. Phys.* **104**, 9932.

[48] Sliwinska-Bartkowiak, M., Dudziak, G., Sikorski, R., Gras, R., Radhakrishnan, R. and Gubbins, K. E. (2001) "Melting/freezing behavior of a fluid confined in porous glasses and MCM-41: Dielectric spectroscopy and molecular simulation", *J. Chem. Phys.* **114**, 950.

[49] Morishige, K. and Iwasaki, H. (2003) "X-ray study of freezing and melting of water confined within SBA-15", *Langmuir* **19**, 2808.

[50] Hung, F. R., Dudziak, G., Sliwinska-Bartkowiak, M. and Gubbins, K. E. (2004) "Freezing/melting behaviour within carbon nanotubes", *Mol. Phys.* **102**, 223.

[51] Hung, F. R., Coasne, B. and Gubbins, K. E. (2006) "Freezing and melting in silica pores of various morphologies", *J. Chem. Phys.*, to be submitted.

Tables:

Table 1. Lennard-Jones potential parameters for the carbon/argon and argon/argon interactions.

Interaction pair	σ (Å)	ε/k_B (K)
Carbon-Carbon	3.36	28.0
Carbon-Argon	3.38	58.0
Argon-Argon	3.41	120.0

Figure captions:

Figure 1. (*left*) Structural model of activated porous carbon CS1000A obtained using a constrained Reverse Monte Carlo method (from Jain *et al.*[15]). The box size is 5.0 nm. The grey sticks represent the C-C bonds. (*right*) Pore size distribution of the activated porous carbon shown on the left.

Figure 2. (*left*) Ar adsorption isotherm at 77.4 K in graphite slit pores: (○) H = 8 Å, (■) H = 10 Å, (Δ) H = 12 Å, and (♦) H = 15 Å. N_0 is the maximum number of adsorbed atoms, while P_0 is the bulk saturation pressure. (*right*) Ar adsorption isotherm at 77.4 K: (○) assembly of unconnected slit pores, (□) activated porous carbon CS1000A. The two samples have the same pore size distribution. N_0 is the maximum number of adsorbed atoms, while P_0 is the bulk saturation pressure.

Figure 3. (*Left*) Isosteric heat of adsorption of Ar at 77.4 K obtained from GCMC simulations: (○) assembly of unconnected slit pores, (□) activated porous carbon CS1000A. The two samples have the same pore size distribution. Adsorbed amounts in abscissa have been normalized to the number of Ar atoms, N_0, when the pores are completely filled. (*Right*) Fluid – wall (closed symbols) and fluid – fluid (open symbols) contributions to the isosteric heat of adsorption of Ar at 77.4 K in microporous carbons. Circles and squares are data for the assembly of unconnected pores and for the activated carbon CS1000A, respectively. The two samples have the same pore size distribution. Adsorbed amounts in abscissa have been normalized to the number of Ar atoms, N_0, when the pores are completely filled.

Figure 4. (*left*) Density profiles of Ar confined at T = 77.4 K in graphite slit pores at the onset of pore filling: H = 7 Å (solid black line), H = 11 Å (solid grey line), and H = 14 Å (dashed black line). z* is the

distance from the center of the pore in reduced units with respect to σ. $\rho^* = \rho\sigma^3$ is the reduced density with respect to σ. (*right*) same as the left graph for $P = P_0$.

Figure 5. (*left*) In plane 2D positional pair correlation function g(r*) for the contact layer of argon confined at $P = 2.0 \times 10^{-4}$ P_0 in a slit graphite pore with $H = 14$ Å. r* is the distance in reduced units with respect to σ. (*right*) In plane 2D positional pair correlation function g(r*) for the contact (black line) and inner (grey line) layers of argon confined at $P = P_0$ in a slit graphite pore with $H = 14$ Å. The g(r*) function for the inner layer has been shifted by +2.0 for the sake of clarity.

Figure 6. (*left*) In plane 2D bond-orientational pair correlation function $G_6(r^*)$ for the contact layer of argon confined at $P = 2.0 \times 10^{-4}$ P_0 in a slit graphite pore with $H = 14$ Å. r* is the distance in reduced units with respect to σ. (*right*) In plane 2D bond-orientational pair correlation function $G_6(r^*)$ for the contact (black line) and inner (grey line) layers of argon confined at $P = P_0$ in a slit graphite pore with $H = 14$ Å. The g(r*) function for the inner layer has been shifted by +0.5 for the sake of clarity.

Figure 7. (*left*) Positional 3D pair correlation function g(r) for Ar confined at 77.4 K in the activated porous carbon CS1000A: $P = 3.0 \times 10^{-5}$ P_0 (dashed black line), $P = 3.0 \times 10^{-3}$ P_0 (solid grey line), $P = P_0$ (solid black line). For the sake of clarity, the g(r) functions for $P = 3.0 \times 10^{-5}$ P_0 and $P = 3.0 \times 10^{-3}$ P_0 have been shifted by +4.0 and +2.0, respectively. (*right*) Distribution of the number of connections per particle for Ar confined in the activated porous carbon CS1000A: (○) $P = 3.0 \times 10^{-5}$ P_0, (□) $P = 3.0 \times 10^{-3}$ P_0, (Δ) $P = P_0$.

Figure 8. Typical configuration of Ar atoms confined at 77.4 K in the activated porous carbon CS1000A: $P = 3.0 \times 10^{-3}$ P_0 (*left*) and $P = P_0$ (*right*). The grey sticks represent the C-C bonds. Grey and

white spheres are Ar atoms that are liquid-like and crystal-like, respectively (see text).

Figure 1.

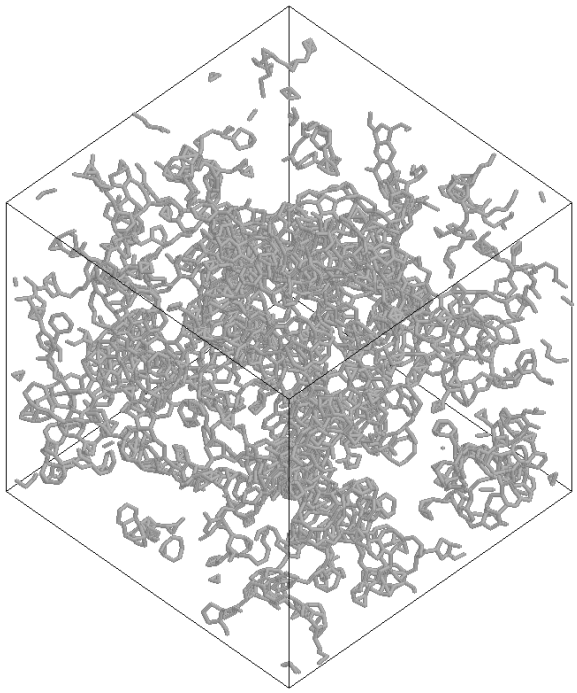

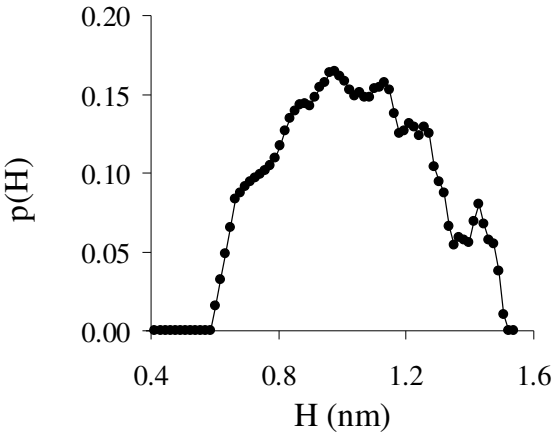

Figure 2.

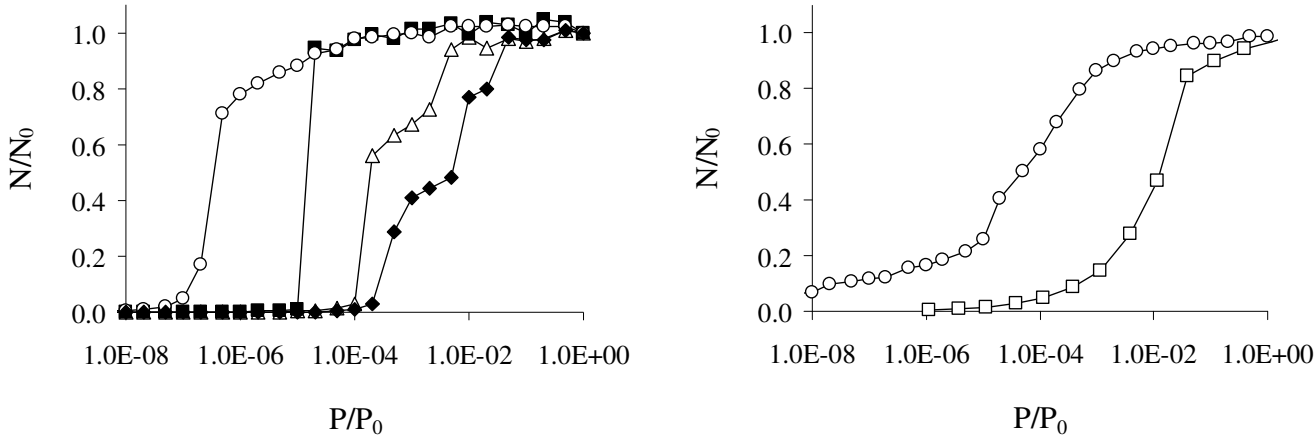

Figure 3.

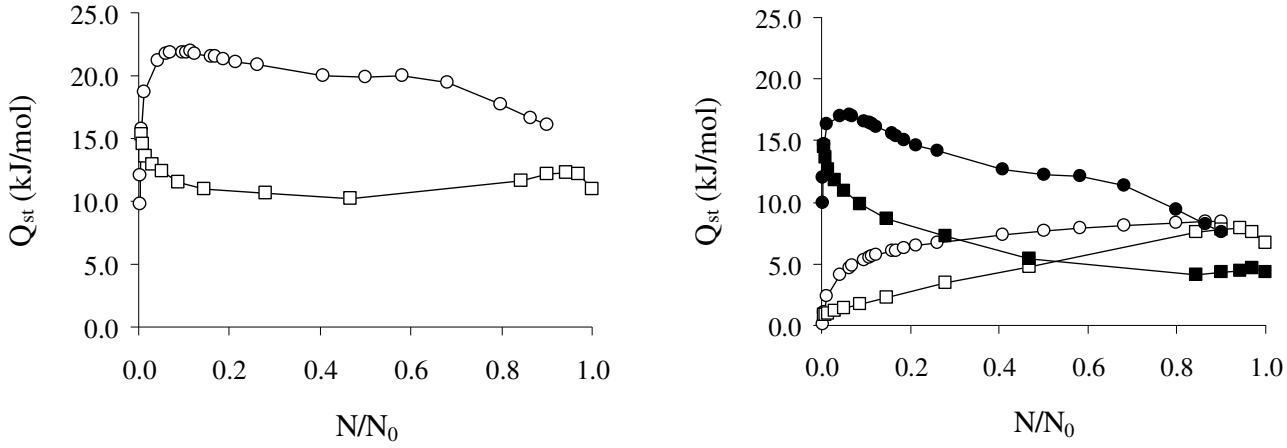

Figure 4.

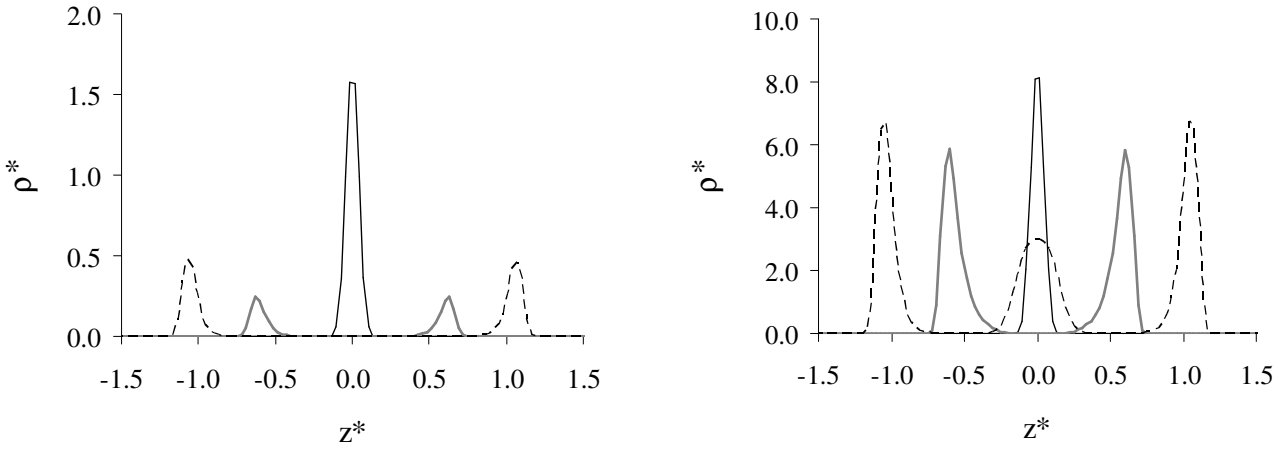

Figure 5.

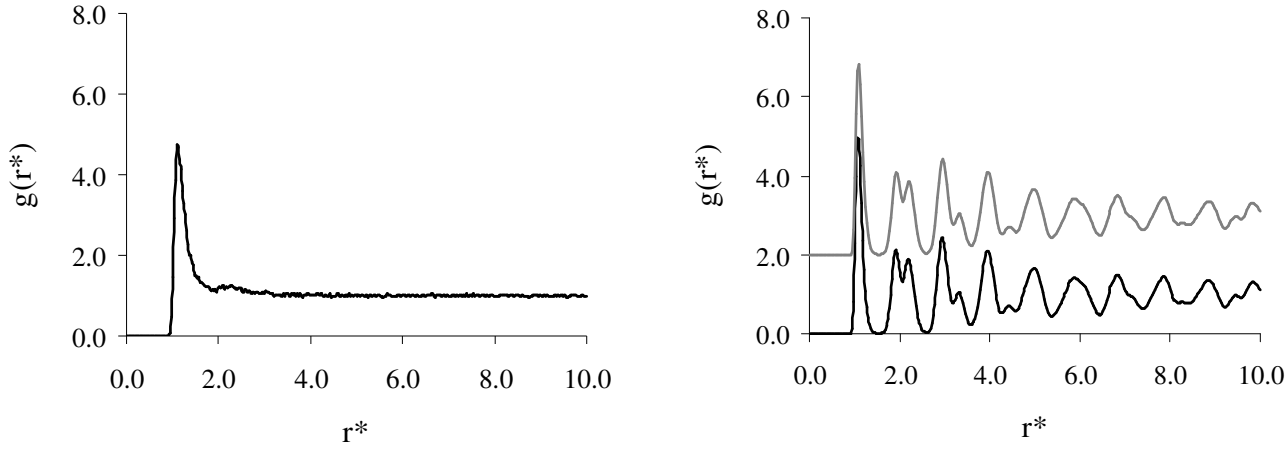

Figure 6.

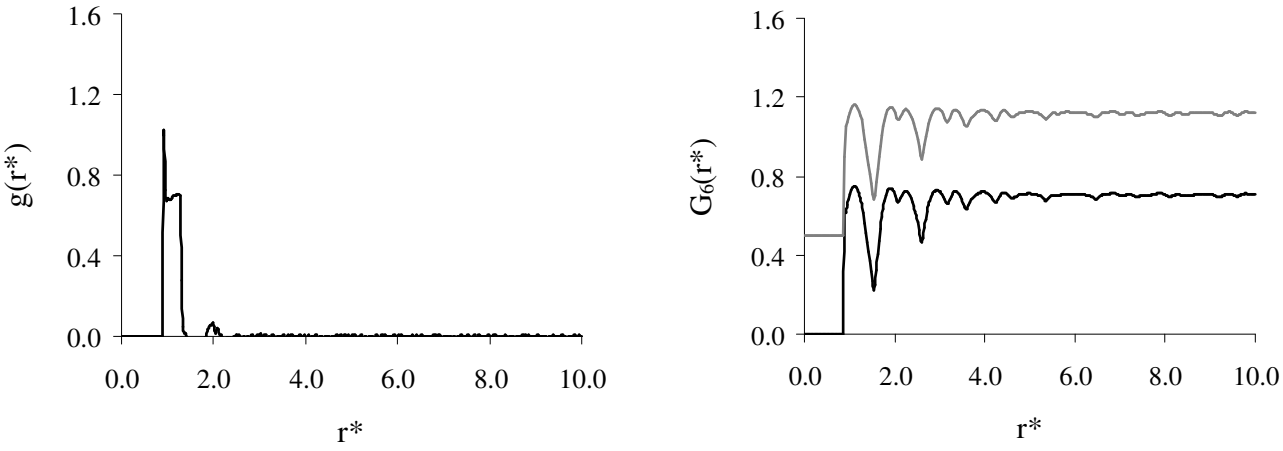

Figure 7.

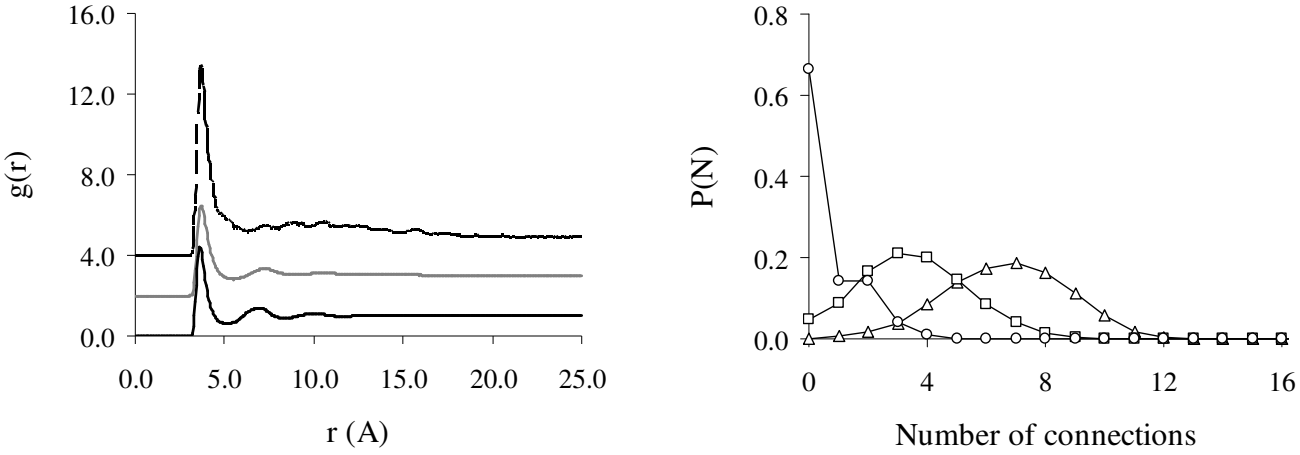

Figure 8.

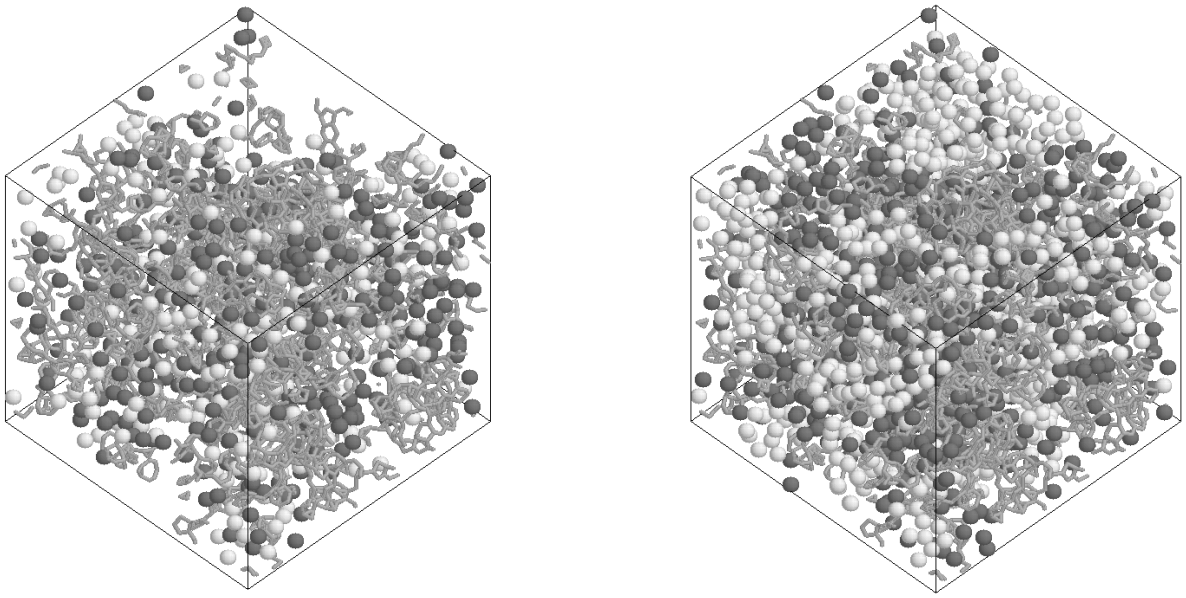

Adsorption and Structure of Argon in Activated Porous Carbons

Benoit Coasne[a,*], Keith E. Gubbins[b], Francisco R. Hung[b,c] and Surendra K. Jain[b]

[a] *Laboratoire de Physicochimie de la Matière Condensée, CNRS (UMR 5617) and Université Montpellier 2, Montpellier, France;* [b] *Center for High Performance Simulations and Department of Chemical and Biomolecular Engineering, North Carolina State University, Raleigh, USA;* [c] *Department of Chemical and Biological Engineering, University of Wisconsin, Madison, USA.*

[*] To whom correspondence should be addressed. E-mail: bcoasne@lpmc.univ-montp2.fr.

Phone: +33 4 67 14 33 78. Fax: +33 4 67 14 42 90.

Abstract. Molecular simulations are used to investigate the adsorption and structure of argon in ordered and disordered models of porous carbons. The ordered porous carbon (model A) is an assembly of regular slit pores of different sizes, while the disordered porous carbon (model B) is a structural model that reproduces the complex pore shape and pore connectivity of saccharose-based porous carbons. The same pore size distribution is used for models A and B so that we are able to estimate, for similar confinement effects, how the disorder of the porous material affects the adsorption and structure of the confined fluid. Adsorption of argon at 77.4 K in the two models is studied using Grand Canonical Monte Carlo simulations. The structure of the confined fluid is analyzed using crystalline bond order parameters and positional or bond orientational pair correlation functions. The filling pressure for the assembly of slit pores is much lower than that for the disordered porous carbon. It is also found that the isosteric heat of adsorption for the ordered porous model overestimates that for the disordered porous model. The results suggest that the agreement between models A and B would be improved if the same density of carbon atoms was used in these two models. Strong layering of Ar is observed at all pressures for model A. The confined phase is composed of liquid-like layers at low pressures, which crystallize into well-defined hexagonal 2D crystals after complete filling of the pores. The structure of argon in the disordered porous carbon strongly departs from that in the slit pore model. Athough its structure remains liquid-like overall, argon confined in model B is composed of both crystalline clusters and amorphous (solid or liquid) nano-domains.

INTRODUCTION

Activated carbons are porous solids with pores having a width of several angstroms. These materials are used in industrial applications as adsorbents for gas separation, air purification, solvent recovery, etc. [1,2,3,4]. From a fundamental point of view, activated porous carbons are used to investigate the effect of confinement, reduced dimension, and surface forces on the phase behavior of fluids [5,6]. Activated porous carbons are obtained by carbonization and chemical or physical activation of some organic precursor (polymer, coconut shell, saccharose, wood, pitch, etc.). The morphological (pore shape) and topological (connected or unconnected pores) features of these materials depend on the conditions of the activation process and on the initial precursor [1,4]. Samples that are obtained from graphitizable precursors such as polymers or pitch fibers are made up of graphene microcrystals [7,8,9,10]; the porosity in these materials consist of defective slit pores that are located between the graphene sheets. On the other hand, samples that are obtained from non-graphitizable precursors such as saccharose exhibit highly disordered pores that are connected [1,4,11].

In most theoretical and molecular simulation studies on fluids confined in porous carbons, the adsorbent is modeled as an assembly of unconnected slit pores having structureless walls (i.e., without surface corrugation). Experimental data of adsorption in porous carbons are usually analyzed on the basis of such a simple model in order to obtain information regarding the pore size distribution, surface area, etc of the real sample [3]. However, it is not clear whether this approximation is justified as most of these adsorbents are made up of connected pores of a complex morphology. Although a few molecular simulation studies have considered models of porous carbons with surface defects or disorder [11,12,13,14,15,16], the effect of pore shape and pore connectivity on the thermodynamics and structure of fluids confined in these materials remains to be clarified. Recent progress in modelling of porous carbons has been achieved through the use of Reverse Monte Carlo (RMC) algorithms [17]. Gubbins and coworkers have applied this technique to obtain structural models of saccharose based porous carbons [11,15,18,19]. Simulated transmission electron microscopy, gas adsorption, and

microcalorimetry for these realistic models were found to be in good agreement with experimental data [16].

In this paper, we report a molecular simulation study of adsorption of argon in ordered and disordered models of activated porous carbons. The ordered porous carbon (model A) is an assembly of regular slit nanopores of different sizes; this model is supposed to be a reasonable approximation for activated carbons obtained from graphitizable precursors. The disordered porous carbon (model B) is a structural model of saccharose-based porous carbon, which was obtained using the RMC method [15]. The disorder in terms of pore shape and pore connectivity in this model is representative of real materials [15]. The same pore size distribution is used for models A and B, so that the comparison between the two set of results allows us to estimate, for similar confinement effects, how the disorder of the porous material affects the adsorption and structural properties of the adsorbate.

Adsorption of argon in the ordered and disordered models of porous carbons was studied using Grand Canonical Monte Carlo (GCMC) simulations. Both the adsorption isotherm (adsorbed amount as a function of the gas pressure) and the isosteric heat of adsorption (differential enthalpy of adsorption as a function of the filling fraction) were calculated in the simulations. The structure of the confined fluid was also determined in the course of the simulations using crystalline bond order parameters and positional or bond orientational pair correlation functions. This paper is organized as follows. The ordered and disordered models of porous carbons and the simulation techniques are described in the second section. Adsorption and structure of argon in the two models of activated porous carbon are discussed in the third section. Concluding remarks and suggestions for future work are presented in the last section of the manuscript.

MODELS AND SIMULATION METHODS

Ordered porous carbons

Ordered porous carbons (model A) were modeled as an assembly of unconnected slit pores having a regular width. The graphite walls in this model are structureless, i.e. without atomic surface corrugation; this approximation is expected to be reasonable for argon as the size of this adsorbate, σ ~ 3.405 Å, is much larger than the spacing between carbon atoms in graphite, D ~ 1.4 Å. The square section of the parallel walls were chosen equal to 20σ × 20σ, which corresponds to 68.1 Å × 68.1 Å. The interaction between the adsorbate atoms and each pore wall was determined using the Steele '10-4-3' potential [20,21]:

$$U_{wf}(z) = 2\pi\rho_w\varepsilon_{wf}\sigma_{wf}^2\Delta\left[\frac{2}{5}\left(\frac{\sigma_{wf}}{z}\right)^{10} - \left(\frac{\sigma_{wf}}{z}\right)^{4} - \left(\frac{\sigma_{wf}^4}{3\Delta(z+0.61\Delta)^3}\right)\right] \quad (1)$$

where z is the distance between the argon atom and the graphite surface. Δ = 3.35 Å is the separation between graphite layers and ρ_w = 0.114 Å^{-3} the atomic density of graphite layers. ε_{wf} and σ_{wf} were calculated by combining the Lennard – Jones parameters for the carbon/carbon [20] and argon/argon [22] interactions using the Lorentz-Berthelot rules [23] (see Table 1).

Disordered porous carbons

The disordered porous carbon (model B) used in this work is shown in Figure 1. This structural model of activated porous carbon obtained after carbonization and activation of pure saccharose has been built by Jain et al. using a constrained RMC technique. This reconstruction method consists of generating atomic configurations that match the structural properties of the real system [17]. The quantity to be minimized in the course of the simulation is:

$$\chi^2 = \sum_{i=1}^{n\exp}\left[S_{sim}(q_i) - S_{\exp}(q_i)\right]^2 \quad (2)$$

where S_{sim} is the simulated structure factor and S_{exp} is the experimental structure factor. Changes in the

atomic configurations are accepted or rejected according to the Metropolis acceptance probability:

$$P_{acc} = \min\left[1, \exp\left\{-\frac{1}{T_\chi}\left(\chi^2_{new} - \chi^2_{old}\right)\right\}\right] \quad (3)$$

where T_χ is a weighting parameter. The uniqueness of structures determined by the RMC method has been questioned in the literature [24]. If many body forces are important in the system (as for carbon materials in which chemical bonding is involved), then it is necessary to include some constraints, representative of these forces, in the RMC method to completely specify the system. Following the previous work by Pikunic et al. [11], appropriate constraints were used to build the realistic model of activated porous carbon considered in this work. The first constraint is that the fraction of atoms in the model having sp^2 hybridization (i.e., coordination number of 3) is centered about this same fraction determined from the experimental composition. The second constraint is that the average C-C-C bond angle, θ, must be equal to $2\pi/3$, as expected for sp^2 hybridization. In the RMC simulation, the difference between the experimental and simulated pair correlation function are simultaneously minimized with the two constraints:

$$\chi^2 = \sum_{i=1}^{n_{\exp}}\left[g_{sim}(r_i) - g_{\exp}(r_i)\right]^2, \quad \delta^2 = \left[\left(\frac{N_3}{N}\right)_{sim} - \left(\frac{N_3}{N}\right)_{target}\right]^2, \quad \psi^2 = \frac{1}{n}\sum_{\theta_i=1}^{n_\theta}\left[\cos(\theta_i) - \cos\left(\frac{2\pi}{3}\right)\right]^2 \quad (4)$$

where $g(r)$ is the radial distribution function for carbon atoms in the material.

In order to improve the quality of the sampling in the RMC simulation, the method was combined with a simulated annealing technique. The latter is a minimization technique that consists of first melting at high temperature the structure to be optimized and then slowly lowering the temperature. Starting with a random initial structure at high temperature, the system runs at this temperature for a large number of moves until it reaches equilibrium; each move consists of randomly selecting and displacing a C atom to

a new position. Then, the temperature is decreased and the system is again allowed to equilibrate. The simulation is complete when no further change is observed upon decrease of the temperature. Full details of the simulation techniques can be found in Refs. [11] and [15].

Grand Canonical Monte Carlo simulations

Argon adsorption in the different models of activated porous carbons was simulated using the GCMC algorithm. The GCMC technique is a stochastic method that simulates a system having a constant volume V (the pore with the adsorbed phase), in equilibrium with an infinite fictitious reservoir of particles imposing its chemical potential μ and its temperature T [25,26,27]. For different values of μ, the absolute adsorption isotherm is determined as an ensemble average of the number of adsorbed atoms *versus* the pressure of the gas reservoir P (the latter is obtained from the chemical potential according to the equation of state for an ideal gas [28]). The adsorption and desorption processes are simulated by increasing and decreasing the chemical potential of the reservoir, respectively; the final configuration obtained from the simulation for a particular chemical potential is the initial configuration for the next point. Periodic boundary conditions were applied for both models A and B in order to avoid finite-size effects. The Ar/Ar interactions were calculated using Lennard-Jones potentials with the parameters reported in Table 1. As mentioned above, interactions between Ar and the slit pore walls for model A were calculated using the 10 – 4 – 3 Steele potential given by equation (1). The interaction of argon atoms with the carbon atoms of the disordered porous material were modeled using a Lennard-Jones potential; the fluid/fluid and fluid/wall parameters were the same as those used for the slit pore model (Table 1). In order to accelerate the simulations in the case of model B, the adsorbate/substrate interaction was calculated by using an energy grid [29]; the potential energy is calculated at each corner of each elementary cube (about $0.025 \times 0.025 \times 0.025$ nm^3). An accurate estimation of the energy is then obtained by a linear interpolation of the grid values. This procedure enables simulation of adsorption in nanoporous media of complex morphology and/or topology without a direct summation over matrix species in the course of GCMC runs [30,31,32,33]. Typical GCMC runs consist of an

equilibration stage of at least 10^5 Monte Carlo steps per particle to equilibrate the system, followed by a production stage of 2.10^5 Monte Carlo steps per particle to obtain averaged data.

RESULTS AND DISCUSSION

Adsorption isotherm and isosteric heat

Argon adsorption in graphite slit pores was studied for 19 pore sizes ranging from H = 6.0 to 15.0 Å; the width difference between two consecutive pore sizes was 0.5 Å. This width range was selected as it covers the pore size distribution for the disordered carbon (see Figure 1). Ar adsorption isotherms at 77.4 K are reported in Figure 2 for the slit pores H = 8, 10, 12 and 15 Å. Adsorbed amounts have been normalized to the maximum number of adsorbed atoms at $P = P_0$. The filling of the slit pores H = 8 and 10 Å occurs at $P = 2.0 \times 10^{-7}\ P_0$ and $1.0 \times 10^{-5}\ P_0$, respectively. These two slit pores accommodate one layer of confined argon after complete filling of the porosity. On the other hand, the adsorption isotherms for the slit pores H = 12 and 15 Å exhibits several steps, which correspond to the filling of different number of layers. For instance, the filling for H = 12 Å starts at $P = 1.0 \times 10^{-4}\ P_0$ with the formation of two layers of confined fluid and ends at $P = 2.0 \times 10^{-3}\ P_0$ with the formation of a third layer within the pore. The filling for H = 15 Å involves a three stage – process with the filling of 3, 4 and 5 layers of argon at $P = 2.0 \times 10^{-4}\ P_0$, $5.0 \times 10^{-3}\ P_0$ and $2.0 \times 10^{-2}\ P_0$, respectively. The dependence of the nature of the filling mechanism on the pore width has been addressed in several recent papers [34,35,36,37]. As expected for adsorption of simple adsorbates in graphite slit pores, we found in general that the filling pressure increases as the pore width increases. However, some exceptions to this rule were observed; for instance, the filling pressure for H = 6 Å, $P = 2.0 \times 10^{-4}\ P_0$, is much larger than that for H = 8 Å, $P = 2.0 \times 10^{-7}\ P_0$, although these two pores accommodate the same number of layers. This result is due to the fact that the wall/fluid interaction energy of an atom in the center of the pore is smaller for H = 6 Å than for H = 8 Å because the atom feels more the repulsive part of the wall/fluid potential in the first case than in the second one (see Ref. [38] for a detailed discussion on the optimal

pore width for a given number of layers).

The Ar adsorption isotherm at 77.4 K for the disordered porous carbon (model B) is shown in Figure 2. We also report the Ar adsorption isotherm for an assembly of unconnected slit pores (model A) having the same pore size as that of model B. The adsorbed amount $N(P/P_0)$ for model A was calculated at a given pressure P/P_0 by:

$$N(P/P_0) = \int_0^\infty n(H, P/P_0) p(H) dH \quad (5)$$

where $p(H)$ is the pore size distribution (see Figure 1) and $n(H, P/P_0)$ the adsorbed amount in the pore of width H. We used a discrete sum in equation (5) instead of an integral, due to the use of a finite number of pore sizes. All the adsorption isotherms shown in Figure 2 have been normalized to the number of adsorbed atoms at $P = P_0$. Both the adsorption isotherms for models A and B are characteristic of adsorption in microporous adsorbents (type I in the IUPAC classification [3]); the filling of the porosity is a reversible process that occurs at very low pressures. The filling of the disordered porous carbon occurs on a range of pressure from $P = 10^{-4} P_0$ up to $P = 4.0 \times 10^{-2} P_0$, while the filling of the slit pores spans over a much larger pressure range from $P = 10^{-8} P_0$ up to $P = 5.0 \times 10^{-3} P_0$. The pressure at which half of the porosity is filled is lower for model A, $P = 5.0 \times 10^{-5} P_0$, than for model B, $P = 10^{-2} P_0$. It is also found that, at all pressures, the adsorbed amount for the assembly of slit pores is larger than that for the disordered carbon. These last results show that the slit pore model significantly understimates the filling pressure of the disordered porous carbon. This finding is in full agreement with our previous work on nitrogen adsorption at 77 K in ordered and disordered porous carbons [13]. As noted in Ref. [13], the difference between the two pore models can be explained by the larger carbon density used in model A, $\rho = 0.114$ Å^{-3}, than that used in model B, $\rho = 0.036$ Å^{-3}. We expect that the agreement between the adsorption isotherms obtained for the ordered and disordered porous carbons can be improved if the same density of carbon atoms is used. However, we have not

attempted to do that because of the important differences in the behavior of the isosteric heat obtained from both models (see below), which will not be eliminated by simply adjusting the density of carbon atoms.

The isosteric heat of adsorption, Q_{st}, as a function of the filling fraction is shown in Figure 3 for the assembly of slit pores and the disordered porous carbon. The latter quantity was calculated in the GCMC simulations from the fluctuations over the energy, *U*, and number of particles, *N*, according to the following formula [25]:

$$Q_{st} = k_B T - \frac{\partial \langle U \rangle}{\partial \langle N \rangle} \sim k_B T - \frac{\langle UN \rangle - \langle U \rangle \langle N \rangle}{\langle N^2 \rangle - \langle N \rangle^2} \qquad (6)$$

For all filling fractions, the isosteric heat of adsorption for the disordered porous carbon is lower than that for the assembly of slit pores. Q_{st} for the slit pore model exhibits a maximum value for $N/N_0 \sim 0.07$ as it first increases from 10 kJ/mol up to 22 kJ/mol and then decreases down to 16 kJ/mol. In contrast, the isosteric heat of adsorption curve for model B is characteristic of adsorption in heterogeneous porous systems as Q_{st} decreases with increasing the filling fraction. This feature is in qualitative agreement with microcalorimetry measurements on disordered porous carbons [16], showing that model B reproduces in a more realistic way the adsorption properties of real porous carbons than model A. We also report in Figure 3 the fluid/wall and fluid/fluid contributions to the total isosteric heat of adsorption for both models A and B. The wall/fluid contribution represents at all filling fractions more than 50% of the total isosteric heat of adsorption. This contribution shows a generally decreasing tendency with increasing N/N_0 as sites of high energy are first filled followed by sites of lower energy. In contrast, the fluid/fluid contribution increases with increasing N/N_0 as the fluid/fluid interaction energy becomes larger. However, it is found that this fluid/fluid contribution slightly decreases at very large filling fractions ($N/N_0 \geq 0.9$) for model B; this result is due to the fact that adsorbed atoms feel the repulsive part of the fluid/fluid interaction at high density (compressibility limit of the fluid). We could not check

this effect of the short range repulsion for model A as fluctuations over the energy and the number of adsorbed atoms at high density were not large enough to get reasonable estimates of the isosteric heat of adsorption. The fluid/fluid contribution of Q_{st} for the slit pore model is always larger than that for the disordered porous carbon. This result is due to the slit pore geometry, which allows the formation of well-structured layers of argon (see below) that are more stable than disordered adsorbate structures. It is found that the fluid/wall contribution to the isosteric heat of adsorption for model A also overestimates that for model B. As mentioned above, this result can be explained by the larger density of carbon walls used in model A, which leads to larger wall/fluid interaction energy.

Structure of the confined fluid

The structure of the confined fluid was analyzed for both models A and B using crystalline bond order parameters, and positional and bond orientational pair correlation functions. Three different sizes, H = 7, 11 and 14 Å, were considered for the slit pore model as they correspond to the smallest, mean, and largest pore size in the disordered porous carbon, respectively. Density profiles of Ar confined at T = 77.4 K are shown in Figure 4 for the slit pores H = 7, 11 and 14 Å. Here z* and ρ* are respectively the reduced distance from the center of the pore and the reduced density with respect to σ. For each pore, we report both the density profile at the onset of pore filling and at the saturated vapor pressure. Significant layering of Ar was observed for all the slit pores as 2D layers are separated by a minimum value of the density, ρ* = 0. This result is due to the strong interaction between argon and the attractive pore walls, which leads to the ordering of the adsorbed phase. For all pressures, the slit pore H = 7 and 11 Å accommodate one and two layers, respectively. On the other hand, the slit pore H = 14 Å accommodates two layers at low pressures and three layers after pore filling. In the latter case, it is found that the peak amplitude for the inner layer is lower than that for the two contact layers (see Figure 4). This result shows that the contact layers are more ordered than the inner layer, due to its stronger interaction with the pore wall. A detailed study of the structure of argon confined in the slit pore H = 14 Å is reported in what follows but similar results were found for the slit pores H = 7 and 11 Å. Following

previous molecular simulation studies on simple fluids in slit pores, the structure of confined argon was investigated by calculating for each layer of adsorbate the in-plane 2D positional g(r) and bond-orientational $G_6(r)$ pair correlation functions [39,40,41,42,43]. The latter measures for each layer *i* the correlations between the local order parameter $\Psi_{6,j}(r)$ at two positions separated by a distance *r*:

$$G_{6.i}(r) = \left\langle \Psi^*_{6,i}(0)\Psi_{6,i}(r) \right\rangle \quad (7)$$

$\Psi_{6,i}(r)$ is the hexagonal bond-order parameter of a particle located at a position **r** in the layer *i* [44,45]:

$$\Psi_{6,i}(\mathbf{r}) = \frac{1}{N_b}\sum_{k=1}^{N_b} \exp\left(i6\theta_k\right) \quad (8)$$

where θ_k is the orientation of the bond angle between the central molecule and each of its N_b nearest neighbors. Correlations within each layer were determined up to a distance of half the size of the simulation box. The g(r) and $G_6(r)$ functions for the contact layer of argon at $P = 2.0 \times 10^{-4}\ P_0$ in the slit pore H = 14 Å are shown Figure 5 and Figure 6. We report only pair correlation functions for the contact layers as the pore H = 14 Å accommodates only two contact layers at this pressure located at the onset of pore filling. We also show in Figure 5 and Figure 6 the g(r) and $G_6(r)$ functions for the contact and inner layers of argon in the same slit pore at $P = P_0$. At $P = 2.0 \times 10^{-4}\ P_0$, the confined layers exhibit a fluid-like behavior as revealed by the g(r) function, which is characteristic of a phase having short-range positional order. This result is confirmed by the very fast decay observed in the $G_6(r)$ function; such a decay is typical of 2D fluid phases, which have short-range orientational order. In contrast, both the contact and inner layers at $P = P_0$ are 2D hexagonal crystals with long-range positional order as can be seen from the features of the g(r) function for this pressure (Figure 5); (i) the amplitude between the first and the second peak is close to 0, (ii) the second peak is split into two secondary peaks, and (iii) the third peak presents a shoulder on its right side. Moreover, the $G_6(r)$ functions at this pressure have a constant average value as expected for hexagonal crystal layers with long-range orientational order

(Figure 6). Analysis of the in-plane 2D pair correlation functions g(r) and $G_6(r)$ was confirmed by calculating for each adsorbate layer *i* the 2D bond-order parameters $\Phi_{6,i}$. We determined $\Phi_{6,i}$ as the average value of the local order parameter $\Psi_{6,i}(r)$ over the entire layer [44,45]:

$$\Phi_{6,i} = \frac{\left| \int \Psi_{6,i}(\mathbf{r})\, d\mathbf{r} \right|}{\int d\mathbf{r}} \qquad (9)$$

$\Phi_{6,i}$ is 1 for a perfect crystal layer having a hexagonal structure (i.e., triangular symmetry) and close to 0 for a liquid layer. At $P = 2.0 \times 10^{-4}\ P_0$, $\Phi_6 = 0.14$ as expected for confined layers having short-ramge orientational order. On the other hand, $\Phi_6 = 0.81$ for the contact and inner layers at $P = P_0$, which confirms that the adsorbate layers have a hexagonal crystal structure with, however, some defects. These results show that argon confined in slit pores at the saturated vapor pressure has a crystalline structure at $T = 77.4$ K, that is lower than the bulk freezing temperature, $T = 83$ K. This finding is consistent with previous molecular simulation studies, which have shown that simple fluids confined in strongly attractive pores crystallize at higher temperature than the bulk [6,39,40,46].

The positional pair correlation function g(r) for Ar confined at 77.4 K in the disordered porous carbon (model B) is shown in Figure 7 for three different pressures $P = 3.0 \times 10^{-5}\ P_0$, $3.0 \times 10^{-3}\ P_0$, and P_0. The filling fractions N/N_0 for these three pressures are 0.05, 0.50 and 1.00, respectively. In contrast to the in-plane 2D g(r) functions used for the slit pore geometry, the functions shown in Figure 7 are 3D pair correlations functions, as no layered structure was observed for argon in the disordered porous carbon (the *x*, *y*, and *z* directions are equivalent for this porous material). For all pressures, the g(r) function of argon confined in model B is characteristic of liquid-like structures as only short – range positional order is observed. It is found that the positional correlations are limited to the first nearest neighbors for the lowest pressure, while they extend to the second and third nearest neighbors for $P = 3.0 \times 10^{-5}\ P_0$ and $3.0 \times 10^{-3}\ P_0$. This change in the range of the correlations indicates that the confined phase presents more short-range structure with increasing filling fraction, although it remains liquid-like overall.

The structure of argon confined in the disordered porous carbon was further characterized by determining its degree of crystalline order. Global crystalline order parameters are not suitable for studying the structure of fluids in the complex porous carbon as the large degree of disorder of the sample prevents the positional and orientational order of the confined phase from being coherent [47]. Thus, instead of global parameters, we used a local order parameter proposed by Ten Wolde et al. [47] to calculate the percentage of atoms that are crystal-like. For each atom *i* of the confined phase, we calculated the 13 normalized parameters $\tilde{q}_{6m}(i)$ that are defined as:

$$\tilde{q}_{6m}(i) = \frac{A}{N_b(i)} \sum_{j=1}^{N_b(i)} Y_{6m}\left(\theta_{ij}, \phi_{ij}\right) \text{ with } m \in [-6,6] \qquad (10)$$

where θ_{ij} and ϕ_{ij} are the polar and azimuthal angles giving the orientation of the vectors joining the atom *i* and each of its $N_b(i)$ neighbors *j*. Y_{6m} are spherical harmonics and A the normalization constant. $\tilde{q}_{6m}(i)$ is a local quantity that depends only on atom *i* and its neighbors *j*. For each pair of nearest neighbors, Ten Wolde et al. defined the following scalar product [47]:

$$\mathbf{q}_6(i) \cdot \mathbf{q}_6(j) = \sum_{m=-6}^{6} \tilde{q}_{6m}(i) \tilde{q}_{6m}(j)^* \qquad (11)$$

Atoms *i* and *j* can be considered "connected" in a coherent manner if the product $\mathbf{q}_6(i) \cdot \mathbf{q}_6(j)$ is larger or equal to 0.5. Ten Wolde et al. have shown that an atom *i* in a 3D environment is crystal-like if it is connected in a coherent manner to at least 7 of its nearest neighbors; this definition ensures that liquid and bcc or fcc crystal structures are unambiguously distinguished [47].

The distribution of the number of connections per Ar particle in the disordered porous carbon was determined for several pressures, $P = 3.0 \times 10^{-5}\ P_0$, $P = 3.0 \times 10^{-3}\ P_0$, and $P = P_0$, from the number of connections for which $\mathbf{q}_6(i) \cdot \mathbf{q}_6(j) \geq 0.5$ (Figure 7). The average number of connections per particle

increases with increasing the pressure from 0.6 at $P = 3.0 \times 10^{-5}\ P_0$ up to 6.7 at $P = P_0$. At the lowest pressure, the confined phase is composed only of liquid-like particles (number of connections < 7). In contrast, the confined phase for $P = 3.0 \times 10^{-3}\ P_0$ and P_0 is composed of both crystal-like and liquid-like adsorbed atoms. We note that, even at the saturating pressure, the average number of connections per particle is much lower than the values expected for FCC and BCC bulk crystals (number of connections ~ 12 and 13, respectively [47]). This result is due to the confinement and the disorder of the porous material, which prevent the formation of any bulk-like regular crystal.

The percentage of Ar atoms that are crystal-like is 0% for $P = 3.0 \times 10^{-5}\ P_0$, 6% for $P = 3.0 \times 10^{-3}\ P_0$, and 54% for $P = P_0$. This result indicates that the confined phase for the two highest pressures corresponds to a mixture of crystalline clusters and amorphous (liquid or solid) regions. This finding strongly departs from what is observed for the slit geometry, where the pore accommodates layers of adsorbate having a well-defined crystalline structure. Our results for the disordered porous carbon are consistent with previous molecular simulations and experiments on molecular fluids in cylindrical silica or carbon pores [48,49,50,51], which have found that the confined fluid does not crystallize but forms an inhomogeneous phase composed of nanocrystallites and amorphous regions. We report in Figure 8 typical atomic configurations of argon confined in the disordered porous carbon at $P = 3.0 \times 10^{-3}\ P_0$ and $P = P_0$ in which we distinguish Ar atoms that are crystal-like and liquid-like.

CONCLUSION

This paper reports a molecular simulation study on adsorption of argon in ordered (model A) and disordered (model B) activated porous carbons. Model A is an assembly of regular slit nanopores, which is representative of graphitizable porous carbons. Model B is a realistic sample of porous carbons obtained from Reverse Monte Carlo; the complex pore shape and pore connectivity of this structural model is representative of materials obtained after carbonization and activation of pure saccharose. Models A and B have the same pore size distribution, which ranges from 6 to 15 Å. Molecular

simulation of argon in these two models of activated porous carbons is used to estimate how the confinement and the disorder of the porous structure affects both the adsorption and the structure of a simple adsorbate. Adsorption of argon at 77.4 K was investigated in the two pore models by means of GCMC simulations. The structure of the confined fluid was analyzed using crystalline bond order parameters and positional or bond orientational pair correlation functions.

Both the Ar adsorption isotherms for the ordered and disordered porous carbon are characteristic of adsorption in microporous adsorbents as the filling mechanism is reversible and occurs at very low pressures. The filling pressure for the assembly of slit pores is found to be much lower than that for the disordered porous carbon, in agreement with our previous work on nitrogen adsorption in similar models of activated porous carbons [13]. It seems that the agreement between models A and B can be improved if the same density of carbon atoms is used for the ordered and disordered models of porous carbons. The isosteric heat of adsorption as a function of the filling fraction exhibits a maximum value for model A, which is not observed for model B. The isosteric heat of adsorption for model B is characteristic of adsorption in heterogeneous porous systems, as it decreases with increasing the filling fraction. It is found that the isosteric heat for the assembly of slit pores is greater than that for the disordered porous carbon. This result can be explained as follows. First, the slit pore geometry allows the formation of well-structured layers of argon, which leads to higher fluid/fluid interactions compared to the disordered porous carbon. In addition, the fluid/wall interaction for the slit pores is greater than that for the complex porous carbon, due to the larger density of the carbon walls used in the first case.

Strong layering of Ar is observed for model A. At low pressures (i.e. at the onset of pore filling), both the positional and bond-orientational pair correlation functions show that the adsorbate is made up of 2D confined layers having a liquid-like structure. However, it is found that these layers transform into 2D hexagonal crystal layers as the pore becomes filled. The structure of argon in the disordered porous carbon strongly departs from that in the slit pores. For all filling fractions, the positional pair correlation function g(r) of Ar confined in this disordered material is characteristic of liquid-like structures as only

short – range positional order is observed. However, except at very low pressures where argon atoms are all liquid-like, the confined phase is a mixture of crystalline clusters and amorphous (solid or liquid) nanodomains. This finding is consistent with previous studies on fluids in cylindrical silica or carbon pores, which have shown that the confined fluid forms an inhomogeneous phase of crystallites and amorphous regions.

Further molecular simulations are needed to corroborate and complete the present study. Starting from well-equilibrated configurations of argon in the disordered porous material, we will investigate the dynamics of the confined phase using Molecular Dynamics simulations for different filling fractions. This will provide useful information regarding the nature of the confined phase, such as its diffusion coefficient and relaxation time. From an experimental point of view, differential scanning calorimetry can be used to corroborate our findings and neutron scattering would allow us to gain insights on the structure and/or the dynamics of the confined phase.

Acknowledgements

We are grateful to Dr. Roland Pellenq (CRMC-N, CNRS – Marseille, France) for very fruitful discussions. We thank the U.S. National Science Foundation for support of this research (grant no. CTS-0211792). This research was performed using supercomputing resources from San Diego Supercomputer Center (NSF/MRAC – CHE050047S), the High Performance Computing Center at North Carolina State University, and the Centre Informatique National de l'Enseignement Superieur at Montpellier (CMC 2017).

[1] Bansal, R. C., Donnet, J. B. and Stoeckli, F. (1988) *Active Carbon* (Marcel Dekker, New York).

[2] Sircar, S., Golden, T. C. and Rao, M. B. (1996) "Activated carbon for gas separation and storage", *Carbon* **34**, 1.

[3] Rouquerol, F., Rouquerol, J. and Sing, K. S. W. (1999) *Adsorption by Powders and Porous Solids* (Academic Press, London).

[4] Bandosz, T. J., Biggs, M. J., Gubbins, K. E., Hattori, Y., Liyama, T., Kaneko, K., Pikunic, J. P. and Thomson, K. T. (2003) "Molecular models of porous carbons", *Chem. Phys. Carbon* **8**, 41.

[5] Gelb, L. D., Gubbins, K. E., Radhakrishnan R. and Sliwinska-Bartkowiak, M. (1999) "Phase separation in confined systems", *Rep. Prog. Phys.* **62**, 1573.

[6] Alba-Simionesco, C., Coasne, B., Dosseh, G., Dudziak, G., Gubbins, K. E., Radhakrishnan, R. and Sliwinska-Bartkowiak, M. (2006) "Effects of confinement on freezing and melting", *J. Phys.: Condens. Matter*, in press.

[7] McEnaney, B. (1988) "Adsorption and structure in microporous carbons", *Carbon* **26**, 267.

[8] March, H. and Walker, P. L. Jr. (1979), In: *Chemistry and Physics of Carbon* (Marcel Dekker, New York) Vol. 15, Chap. 3.

[9] Mays, T. J. (1999) In: *Carbon Materials for Advanced Technologies* (Pergamon, Amsterdam), Chap. 3.

[10] Huang, Z. H., Kang, F., Huang, W., Yang, J. B., Liang, K. M., Cui, M. L. and Cheng, Z. (2002) "Pore structure and fractal characteristics of activated carbon fibers characterized by using HRTEM", *J. Coll. and Interf. Sci.* **249**, 453.

[11] Pikunic, J., Clinard, C., Cohaut, N., Gubbins, K. E., Guet, J. M., Pellenq, R. J. –M., Rannou, I. and Rouzaud, J. –N. (2003) "Structural modeling of porous carbons: constrained reverse Monte Carlo method", *Langmuir* **19**, 8565.

[12] Striolo, A., Gubbins, K. E., Chialvo, A. A. and Cummings, P. T. (2005) "The effect of pore connectivity on water adsorption isotherms in non-activated graphitic nanopores", *Adsorption* **11**, 337.

[13] Coasne, B., Pikunic, J. P., Pellenq, R. J.-M. and Gubbins, K. E. (2003) "Comparison between adsorption in pores of a simple geometry and realistic models of porous materials", *Proc. Mat. Res. Soc.* **P8.5**.

[14] Biggs, M. J., Buts, A. and Williamson, D. (2004) "Molecular simulation evidence for solidlike adsorbate in complex carbonaceous micropore structures", *Langmuir* **20**, 5786.

[15] Jain, S. K., Pikunic, J. P., Pellenq, R. J. –M. and Gubbins, K. E. (2005) "Effects of activation on the structure and adsorption properties of a nanoporous carbon using molecular simulation", *Adsorption* **11**, 355.

[16] Pikunic, J. P., Llewellyn, P., Pellenq, R. J. –M. and Gubbins, K. E. (2005) "Argon and nitrogen adsorption in disordered nanoporous carbons: simulation and experiment", *Langmuir* **21**, 4431.

[17] McGreevy, R. L. and Pusztai, L. (1988) "Reverse Monte Carlo Simulation: A new technique for the determination of disordered structures", *Mol. Sim.* **1**, 359.

[18] Thomson, K. T. and Gubbins, K. E. (2000) "Modeling structural morphology of microporous carbons by reverse Monte Carlo", *Langmuir* **16**, 5761.

[19] Jain, S. K., Fuhr, J., Pellenq, R. J. –M., Pikunic, J. P., Bichara, C. and Gubbins, K. E. (2005) "Stability study of porous carbon structures obtained from reverse Monte Carlo using tight binding and bond order Hamiltonians", *Studies in Surface Science and Catalysis*, in press.

[20] Steele, W. A. (1973) "The physical interaction of gases with crystalline solids", *Surf. Sci.* **36**, 317.

[21] Steele, W. A. (1974) *The Interaction of Gases with Solid* Surfaces (Pergamon Press, Oxford).

[22] Streett, W. B. and Staveley, L. A. K. (1967) "Calculation on a corresponding states basis of the volume change on mixing simple liquids", *J. Chem. Phys.* **47**, 2449.

[23] Rowlinson, J. S. (1982) *Liquids and Liquid Mixtures* (Butterworth Scientific, London).

[24] Evans, R. (1990) "Comment on Reverse Monte Carlo Simulation", *Mol. Sim.* **4**, 409.

[25] Nicholson, D. and Parsonage, N. G. (1982) *Computer Simulation and the Statistical Mechanics of Adsorption* (Academic Press, New York).

[26] Allen, M. P., Tildesley, D. J. (1987) *Computer Simulation of Liquids* (Oxford, Clarendon).

[27] Frenkel, D. and Smit, B. (2002) *Understanding Molecular Simulation: From Algorithms to Applications*, 2nd Ed. (Academic Press, London).

[28] D. A. Kofke (1993) "Direct evaluation of phase coexistence by molecular simulation via integration along the saturation line", *J. Chem. Phys.* **105**, 405.

[29] Pellenq, R. J. –M. and Nicholson, D. (1995) "Grand ensemble Monte Carlo simulation of simple molecules adsorbed in silicalite-I zeolite", *Langmuir* **11**, 1626.

[30] Coasne, B. and Pellenq, R. J. –M. (2004) "A grand canonical Monte Carlo study of capillary condensation in mesoporous media: effect of the pore morphology and topology", *J. Chem. Phys.* **121**, 3767.

[31] Coasne, B., Gubbins, K. E. and Pellenq, R. J. –M. (2004) "A grand canonical Monte Carlo study of adsorption and capillary condensation phenomena in nanopores of various morphologies and topologies: testing the BET and BJH characterization methods", *Part. Part. Syst. Charact. 21*, 149.

[32] Gelb, L. D. and Gubbins, K. E. (1998) "Characterization of porous glasses: simulation models, adsorption isotherms, and the Brunauer-Emmett-Teller analysis method", *Langmuir* **14**, 2097.

[33] Pellenq, R. J. –M. and Levitz, P. E. (2002) "Capillary condensation in a disordered mesoporous medium: a grand canonical Monte Carlo study", *Mol. Sim.* **100**, 2059.

[34] Ayappa, K. G. and Ghatak, C. (2002) "The structure of frozen phases in slit nanopores: A grand canonical Monte Carlo study", *J. Chem. Phys.* **117**, 5373.

[35] Bock, H., Gubbins, K. E. and Ayappa, K. G. (2005) "Solid/solid phase transitions in confined thin films: A zero temperature approach", *J. Chem. Phys.* **122**, 094709.

[36] Patrykiejew, A., Salamacha, L. and Sokolowski, S. (2003) "On the structure of Lennard-Jones fluids confined in crystalline slitlike pores", *J. Chem. Phys.* **118**, 1891.

[37] Camara, L. G. and Bresme, F. (2003) "Molecular Dynamics simulations of crystallization under confinement at triple point conditions", *J. Chem. Phys.* **119**, 2792.

[38] Do, D. D. and Do, H. D. (2003) "Refined method of potential enhancement in the equilibria characterization of activated carbon. Comparison with GCMC and DFT", *Langmuir* **19**, 8302.

[39] Radhakrishnan, R. and Gubbins, K. E. (1999) "Free energy studies of freezing in slit pores: an order parameter approach using Monte Carlo simulation", *Mol. Phys.* **96**, 1249.

[40] Radhakrishnan, R., Gubbins, K. E. and Sliwinska-Bartkowiak, M. (2002) "Global phase diagrams for freezing in porous media", *J. Chem. Phys.* **116**, 1147.

[41] Coasne, B., Czwartos, J., Gubbins, K. E., Hung, F. R. and Sliwinska-Bartkowiak, M. (2004) "Freezing and melting of binary mixtures confined in a nanopore", *Mol. Phys.* **102**, 2149.

[42] Coasne, B., Czwartos, J., Gubbins, K. E., Hung, F. R. and Sliwinska-Bartkowiak, M. (2005) "Freezing of mixtures confined in a slit nanopore", *Adsorption* **11**, 301.

[43] Hung, F. R., Coasne, B., Gubbins, K. E., Santiso, E. E., Siperstein, F. R. and Sliwinska-Bartkowiak, M. (2005) "Molecular modeling of freezing of simple fluids confined within carbon nanotubes", *J. Chem. Phys.* **122**, 144706.

[44] Halperin, B. I. and Nelson, D. R. (1978) "Theory of two dimensional melting", *Phys. Rev. Lett.* **41**, 121; Nelson, D. R. and Halperin, B. I. (1979) "Dislocation – mediated melting in two dimensions", *Phys. Rev. B* **19**, 2457.

[45] Strandburg, K. J. (1988) "Two – dimensional melting", *Rev. Mod. Phys.* **60**, 161.

[46] Radhakrishnan, R., Gubbins, K. E., Watanabe, A. and Kaneko, K. (1999) "Freezing of simple fluids in microporous activated carbon fibers: comparison of simulation and experiment", *J. Chem. Phys.* **111**, 9058.

[47] ten Wolde, P. R., Ruiz-Montero, M. J. and Frenkel, D. (1996) "Numerical calculation of the rate of crystal nucleation in a Lennard-Jones system at moderate undercooling", *J. Chem. Phys.* **104**, 9932.

[48] Sliwinska-Bartkowiak, M., Dudziak, G., Sikorski, R., Gras, R., Radhakrishnan, R. and Gubbins, K. E. (2001) "Melting/freezing behavior of a fluid confined in porous glasses and MCM-41: Dielectric spectroscopy and molecular simulation", *J. Chem. Phys.* **114**, 950.

[49] Morishige, K. and Iwasaki, H. (2003) "X-ray study of freezing and melting of water confined within SBA-15", *Langmuir* **19**, 2808.

[50] Hung, F. R., Dudziak, G., Sliwinska-Bartkowiak, M. and Gubbins, K. E. (2004) "Freezing/melting behaviour within carbon nanotubes", *Mol. Phys.* **102**, 223.

[51] Hung, F. R., Coasne, B. and Gubbins, K. E. (2006) "Freezing and melting in silica pores of various morphologies", *J. Chem. Phys.*, to be submitted.

Tables:

Table 1. Lennard-Jones potential parameters for the carbon/argon and argon/argon interactions.

Interaction pair	σ (Å)	ε/k_B (K)
Carbon-Carbon	3.36	28.0
Carbon-Argon	3.38	58.0
Argon-Argon	3.41	120.0

Figure captions:

Figure 1. (*left*) Structural model of activated porous carbon CS1000A obtained using a constrained Reverse Monte Carlo method (from Jain *et al.*[15]). The box size is 5.0 nm. The grey sticks represent the C-C bonds. (*right*) Pore size distribution of the activated porous carbon shown on the left.

Figure 2. (*left*) Ar adsorption isotherm at 77.4 K in graphite slit pores: (○) H = 8 Å, (■) H = 10 Å, (Δ) H = 12 Å, and (♦) H = 15 Å. N_0 is the maximum number of adsorbed atoms, while P_0 is the bulk saturation pressure. (*right*) Ar adsorption isotherm at 77.4 K: (○) assembly of unconnected slit pores, (□) activated porous carbon CS1000A. The two samples have the same pore size distribution. N_0 is the maximum number of adsorbed atoms, while P_0 is the bulk saturation pressure.

Figure 3. (*Left*) Isosteric heat of adsorption of Ar at 77.4 K obtained from GCMC simulations: (○) assembly of unconnected slit pores, (□) activated porous carbon CS1000A. The two samples have the same pore size distribution. Adsorbed amounts in abscissa have been normalized to the number of Ar atoms, N_0, when the pores are completely filled. (*Right*) Fluid – wall (closed symbols) and fluid – fluid (open symbols) contributions to the isosteric heat of adsorption of Ar at 77.4 K in microporous carbons. Circles and squares are data for the assembly of unconnected pores and for the activated carbon CS1000A, respectively. The two samples have the same pore size distribution. Adsorbed amounts in abscissa have been normalized to the number of Ar atoms, N_0, when the pores are completely filled.

Figure 4. (*left*) Density profiles of Ar confined at T = 77.4 K in graphite slit pores at the onset of pore filling: H = 7 Å (solid black line), H = 11 Å (solid grey line), and H = 14 Å (dashed black line). z* is the

distance from the center of the pore in reduced units with respect to σ. $\rho^* = \rho\sigma^3$ is the reduced density with respect to σ. (*right*) same as the left graph for $P = P_0$.

Figure 5. (*left*) In plane 2D positional pair correlation function g(r*) for the contact layer of argon confined at $P = 2.0 \times 10^{-4}\ P_0$ in a slit graphite pore with $H = 14$ Å. r* is the distance in reduced units with respect to σ. (*right*) In plane 2D positional pair correlation function g(r*) for the contact (black line) and inner (grey line) layers of argon confined at $P = P_0$ in a slit graphite pore with $H = 14$ Å. The g(r*) function for the inner layer has been shifted by +2.0 for the sake of clarity.

Figure 6. (*left*) In plane 2D bond-orientational pair correlation function $G_6(r^*)$ for the contact layer of argon confined at $P = 2.0 \times 10^{-4}\ P_0$ in a slit graphite pore with $H = 14$ Å. r* is the distance in reduced units with respect to σ. (*right*) In plane 2D bond-orientational pair correlation function $G_6(r^*)$ for the contact (black line) and inner (grey line) layers of argon confined at $P = P_0$ in a slit graphite pore with $H = 14$ Å. The g(r*) function for the inner layer has been shifted by +0.5 for the sake of clarity.

Figure 7. (*left*) Positional 3D pair correlation function g(r) for Ar confined at 77.4 K in the activated porous carbon CS1000A: $P = 3.0 \times 10^{-5}\ P_0$ (dashed black line), $P = 3.0 \times 10^{-3}\ P_0$ (solid grey line), $P = P_0$ (solid black line). For the sake of clarity, the g(r) functions for $P = 3.0 \times 10^{-5}\ P_0$ and $P = 3.0 \times 10^{-3}\ P_0$ have been shifted by +4.0 and +2.0, respectively. (*right*) Distribution of the number of connections per particle for Ar confined in the activated porous carbon CS1000A: (○) $P = 3.0 \times 10^{-5}\ P_0$, (□) $P = 3.0 \times 10^{-3}\ P_0$, (Δ) $P = P_0$.

Figure 8. Typical configuration of Ar atoms confined at 77.4 K in the activated porous carbon CS1000A: $P = 3.0 \times 10^{-3}\ P_0$ (*left*) and $P = P_0$ (*right*). The grey sticks represent the C-C bonds. Grey and

white spheres are Ar atoms that are liquid-like and crystal-like, respectively (see text).

Figure 1.

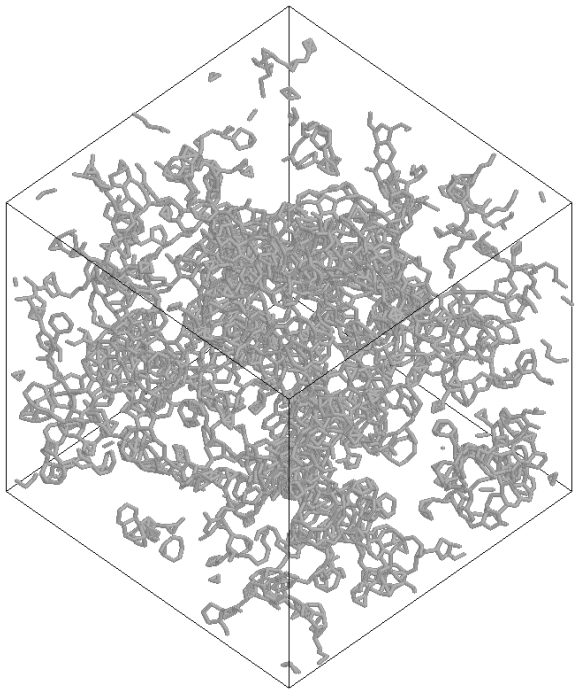

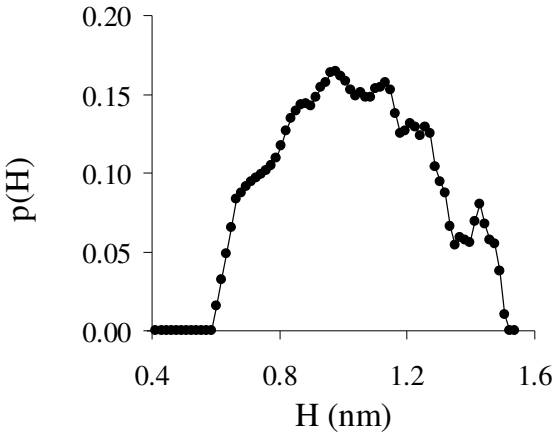

Figure 2.

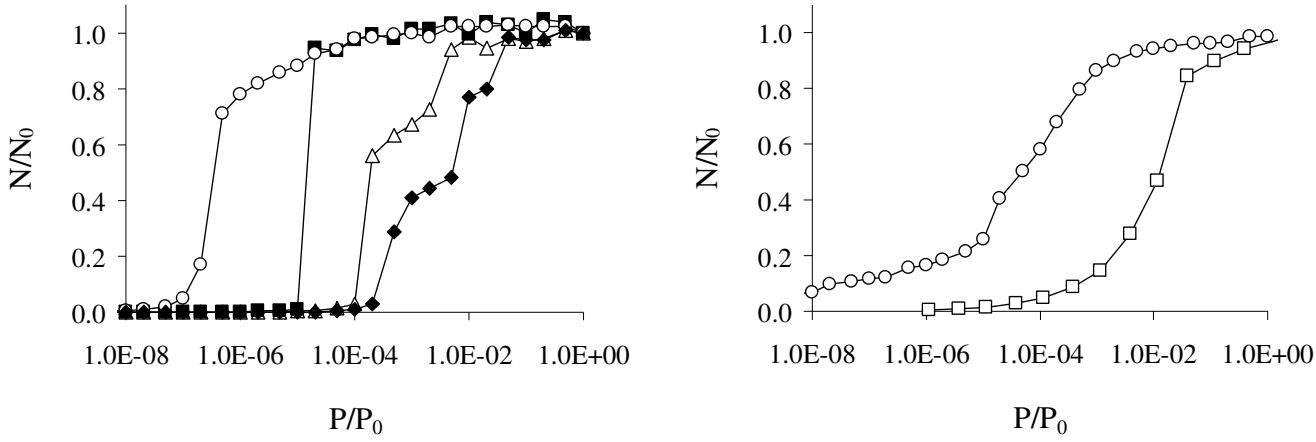

Figure 3.

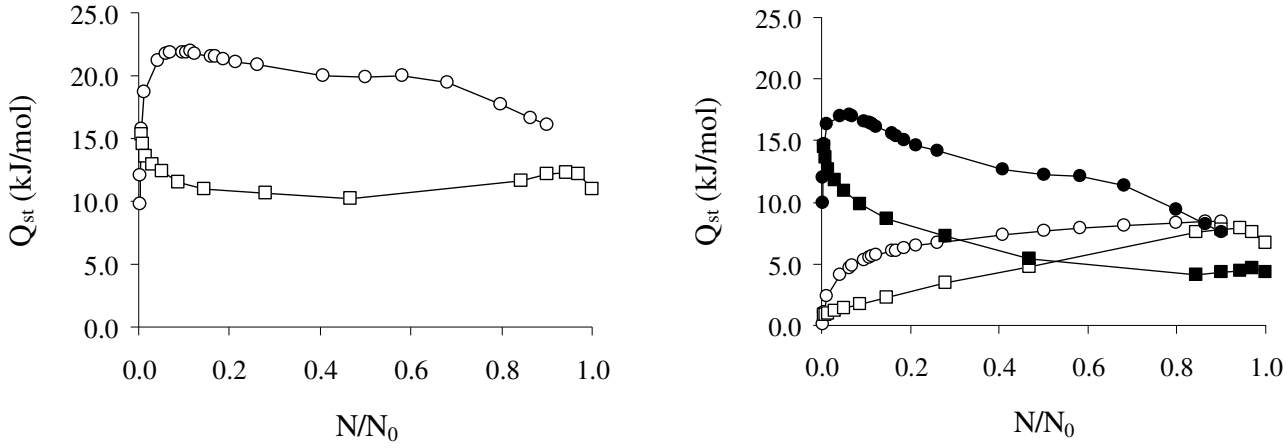

Figure 4.

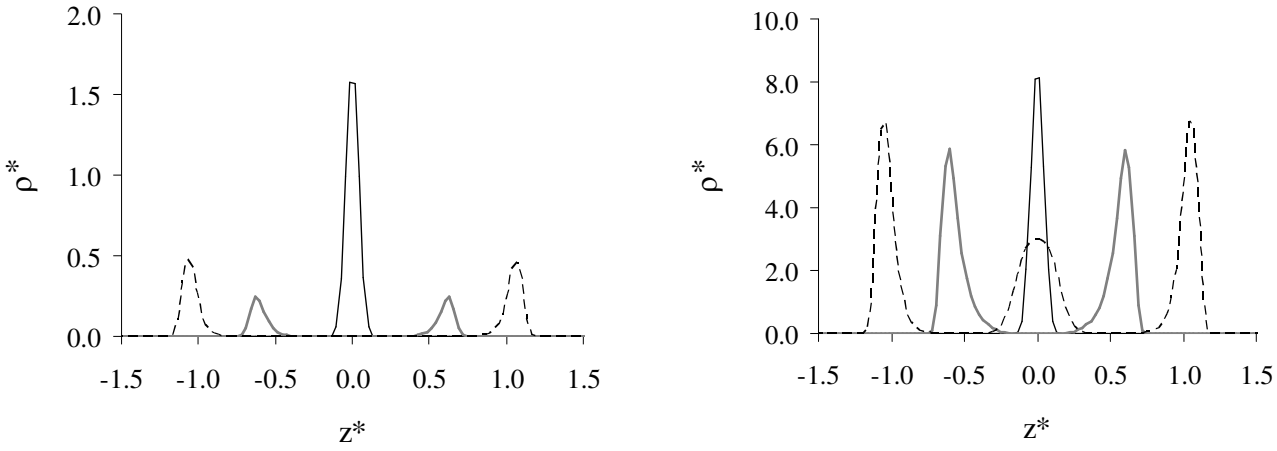

Figure 5.

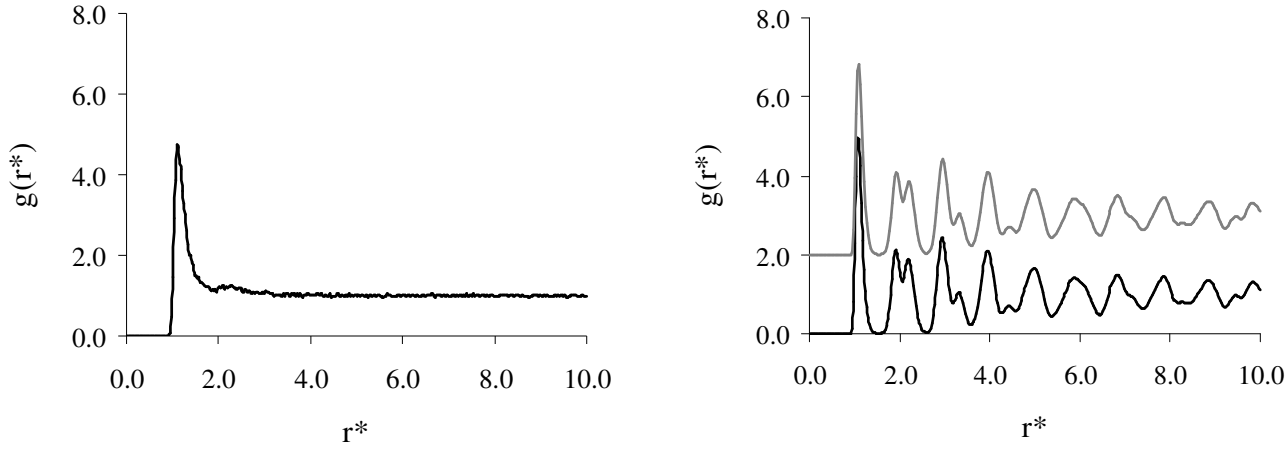

Figure 6.

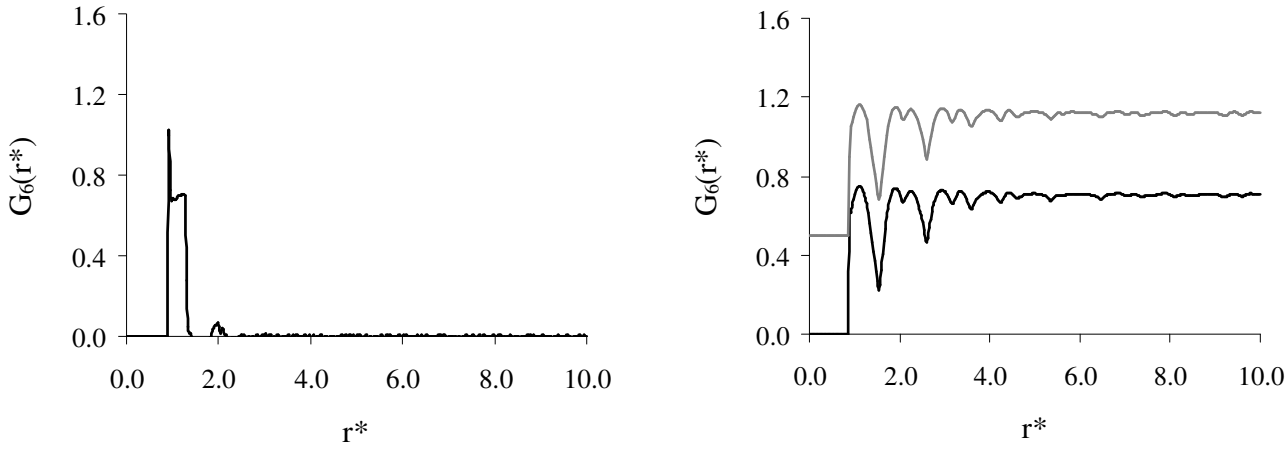

Figure 7.

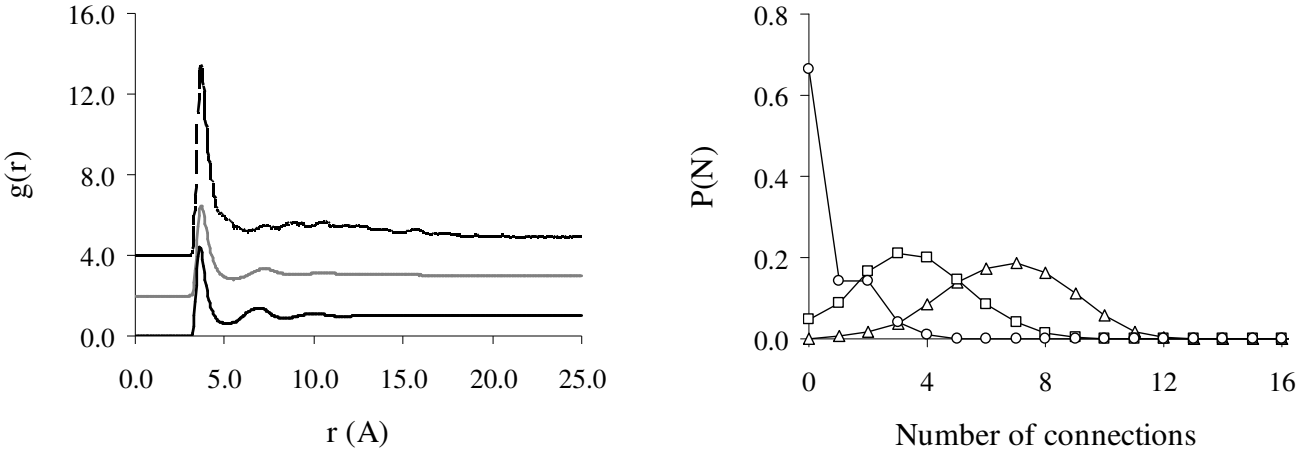

Figure 8.